

Anomalous size–dependence of interfacial
profiles between coexisting phases
of polymer mixtures in thin film geometry:
A Monte–Carlo simulation

**Andreas Werner, Friederike Schmid, Marcus Müller,
and Kurt Binder**

*Institut für Physik, Johannes Gutenberg Universität Mainz
Staudinger Weg 7, D-55099 Mainz, Germany*

February 24, 2018

to be appear in JCP, 15 Nov 1997

Abstract

The interfacial profile between coexisting phases of a binary mixture (A,B) in a thin film of thickness D and lateral linear dimensions L depends sensitively on both linear dimensions and on the nature of boundary conditions and statistical ensembles applied. These phenomena generic for systems in confined geometry are demonstrated by Monte-Carlo simulations of the bond fluctuation model of symmetric polymer mixtures, using chains containing $N_A = N_B = N = 32$ effective monomers connected by effective bonds with an attractive interaction between monomers of the same type and a repulsive interaction between different types. We use short range potentials at the walls, the right wall favoring A monomers and the left wall B monomers. Periodic boundary conditions are applied in the directions parallel to the walls. Both the canonical and semi-grand-canonical ensemble are studied. We argue that the latter case is appropriate for experiments with a lateral resolution L much less than the actual lateral sample size, in thermal equilibrium. In the canonical ensemble, the interfacial width w increases (from small values which are of the same order as the “intrinsic profile”) like $w \propto \sqrt{D}$, before a crossover to a saturation value w_{max} ($w_{max}^2 \propto \ln L$) sets in. In the semi-grand-canonical ensemble, however, one finds the same widths $w \propto \sqrt{D}$ as in the canonical ensemble for not too large L , while for large L the interfacial profile is smeared out over a finite fraction of the film thickness ($w \propto D$ for $D \rightarrow \infty$). We discuss the implications of these findings for the interpretation of both simulations and experiments.

1 Introduction

Since van der Waals' famous treatment of the interface between coexisting fluid and gas, calculations and measurements of interfacial profiles between coexisting phases have remained a particular challenge [1, 2, 3, 4, 5]. Van der Waals type mean field theories were extended to mixtures by Cahn and Hilliard [6], as well as to more complex systems such as polymer solutions [7], polymer blends [8, 9, 10], microemulsions [11, 12], etc. These theories, but also more complex ones such as the self-consistent field approach to strongly segregated polymer mixtures [13, 14, 15, 16, 17, 18, 19, 20, 21, 22] consider a hypothetical "intrinsic" profile that is neither directly accessible by experiment nor by computer simulation. I.e., both in experiment and in simulations these "intrinsic" profiles — if they have a well-defined meaning at all — are broadened by fluctuations (such as capillary waves [19, 20, 23] which can be modelled by harmonic displacements of the local interface position [1, 2, 3, 4]), but this broadening is also limited by the geometry of the (finite !) system that is considered and affected by forces due to the boundaries of the system. In fact, the latter may give rise to interface binding/unbinding phenomena ("wetting" [24, 25, 26, 27, 28, 29, 30]), and the associated fluctuations do have a strong effect on the observable average interfacial profiles [31, 32, 33, 34, 35]. (Note that external potentials such as gravity, which clearly limit interfacial fluctuations in liquid-gas systems, are disregarded here throughout.)

There are numerous examples in the literature, both in experiment (e.g. on polymer mixtures [37, 38]) and simulation (ranging from lattice gas models [39] to the water-vapor interface [40]) where this fluctuation broadening of interfacial profiles is disregarded and the resulting interfacial width is interpreted as if the intrinsic width were obtained. Recent work [34], however, indicates that such an approach may yield rather misleading results !

Fig.1 sketches the $L \times L \times D$ geometries that are typically used in simulations [23, 32, 33, 34, 35, 39, 40] and experiments [34, 37, 38]. L is the linear dimension parallel to the interface(s), D perpendicular to the interface(s). Fig.1a shows a system with a single interface between two demixed phases using either hard walls as boundary condition normal to the interface (left part) or "antiperiodic" boundary conditions (i.e., an A monomer leaving the right boundary of the simulation box reenters at the left boundary as a B monomer, and vice versa; right part). This antiperiodic boundary condition is particular useful for strictly symmetrical mixtures where two species A,B intrinsically are not different apart from their "label", and thus one can achieve a geometry with a single interface and no disturbing effects due to external walls. If periodic boundary conditions are used in all three directions, the system must contain two interfaces (Fig.1b). We emphasize that the concentration profile (and hence also its width w) obtained in these situations depends both on D and on L , and in general may differ appreciably from any sensibly defined intrinsic profile ! The present paper intends to study these dependences for a simple model system that is nevertheless close to physical systems of practical interest, namely polymer mixtures [19, 34, 37, 38]. Experiments are done in the geometry of Fig.1c and encounter closely related problems of interpretation as the simulations as will be explained below.

While in the thermodynamic limit the different ensembles of statistical mechanics yield equivalent results, this is not true in systems which have all their linear dimensions

finite [41]. Considering binary (A,B) mixtures at constant density, we may deal either with the canonical ensemble where the average volume fraction $\bar{\Phi}$ of species A is held fixed (if $\bar{\rho}_A, \bar{\rho}_B$ are the average densities of A particles/B particles in the system, then $\bar{\Phi}_A = \bar{\Phi} = \bar{\rho}_A/(\bar{\rho}_A + \bar{\rho}_B)$, and $\bar{\Phi}_B = 1 - \bar{\Phi} = \bar{\rho}_B/(\bar{\rho}_A + \bar{\rho}_B)$ being the volume fraction of species B) or with the semi-grand-canonical ensemble where the chemical potential difference $\Delta\mu$ between A and B is held fixed. Note that in the left part of Fig.1a the use of the canonical ensemble suppresses the fluctuation of the average position of the interface — e.g. for $\bar{\Phi} = 1/2$ and “antisymmetric” walls acting on a “symmetric” mixture [42] (as considered here and in Refs. [32, 33, 39]) the average position of the interface is fixed in the middle of the film, $z = D/2$. (We disregard here the case [31, 32, 33] of temperatures below the transition temperature $T_c(D)$ of the interface localization–delocalization transition where the interface is bound either to the left or the right wall and $\bar{\Phi} = 1/2$ is maintained only via a lateral inhomogeneity, i.e., formation of domains separated by interfaces running perpendicular to the walls [43].) In contrast, using the semi-grand-canonical ensemble, $\bar{\Phi}$ and hence the average interface positions are fluctuating and, in particular for small L , this fluctuation of the average interface position may even be more important than local distortions of the interface. Naturally, one has to be careful in the interpretation of experiments, too: While the canonical ensemble is appropriate for a discussion on the length scale L_{sample} comprising the total sample, this is not true if the measurement is done with a technique characterized by a length scale L of lateral resolution with $L \ll L_{sample}$ (Fig.1c). The condition $\bar{\Phi} = const$ fixes the average interface position on the length scale L_{sample} , but it clearly does not fix it on the length scale L that is probed. This is the case for experiments where interfacial properties are measured “in situ” in the melt phase [44]. We may consider the slab of width L that is measured as a “subsystem” in a statistical sense that can exchange A,B particles freely by diffusion with the rest of the system. This acts as a reservoir, in thermal equilibrium, and hence the semi-grand-canonical ensemble applies. Implicit in this interpretation is the assumption that the time constant of the measurement is large enough such that one measures not just a kind of “snapshot” of the interfacial configuration, but carries out a meaningful statistical average in thermal equilibrium.

For the fully periodic system [35, 40] (Fig.1b), on the other hand, semi-grand-canonical techniques are inappropriate since then the two-phase configuration shown is at best metastable: If one simulated long enough, the two interfaces would meet and annihilate each other, and either the A-rich domain or the B-rich domain would vanish altogether. The condition $\bar{\Phi} = const$ in the canonical ensemble and fixing the center of mass of the B-rich phase then suppresses also fluctuations of the average interface positions. Finally, in the antiperiodic case there is a clear translational invariance; no origin at the z-axis is distinguished except by the location of the interface itself. Then it is natural to record all information in a moving frame: In each configuration that is analyzed the point $z = 0$ is chosen to coincide with the interface position averaged in x,y directions [23, 45]. Even in the semi-grand-canonical ensemble, the fluctuation of the average interface position is thus eliminated per construction.

In the present paper we shall restrict our attention to the case of a single interface confined between “antisymmetric” walls (i.e., the left part of Fig.1a) since this situation is closest to the experimental one (Fig.1c), studying the finite size effects both in the

canonical and the semi-grand-canonical case. We anticipate, however, that many of our findings carry over qualitatively to the other cases (antiperiodic boundary conditions in Fig.1a, periodic boundary conditions in Fig.1b) as well.

In the next section, we define the model that is used in our study and make a few remarks on the simulation technique. Sec.3 briefly reviews the theoretical background, while Sec.4 gives our results on interfacial profiles and interfacial widths and discusses the correlation function of interfacial fluctuations in directions parallel to the walls and the associated correlation length ξ_{\parallel} . Sec.5 describes a test of capillary wave concepts. Finally, Sec.6 summarizes our conclusions.

2 Model and simulation technique

Since we desire to make as close contact as possible with experiments on polymer mixtures confined in thin film geometry, where size effects as discussed here have already been observed [34, 47], we study a coarse-grained model for a symmetric polymer mixture, extending previous studies of the bond fluctuation model [48] on the simple cubic lattice [22, 23, 49, 50, 51]. We summarize here only very briefly some key features [52] of this well studied model: One integrates $n = 3 - 5$ chemical bonds along the backbone of a real polymer chain into one effective bond, whose length is allowed to fluctuate between the following values: $2, \sqrt{5}, \sqrt{6}, 3, \sqrt{10}$, all lengths being measured in units of the lattice spacing. This variation in the bond length is not only computationally advantageous [49, 52, 53], but also physically reasonable as a result of the internal degrees of freedom of the combined $3 - 5$ original chemical bonds. Furthermore, the 87 different bond angles between subsequent effective bonds approximate properties of continuum models already rather closely. These effective bonds are joined at effective monomers, each blocking all 8 sites of an elementary cube from further occupation. We work at a volume fraction $\Phi_b = 1/2$ of occupied lattice sites, which corresponds to a dense melt [53], i.e., the density of effective monomers is $\rho_b = 1/16$ in our units. For consistency with previous work [23] where interfaces for the antiperiodic boundary conditions (Fig.1a, right part) were studied we choose here a chain length $N = 32$, which hence corresponds to a degree of polymerization $N_p = nN \approx 96 - 160$. For this choice, the radius of gyration R_g of the chains is about $R_g \approx 7$ lattice spacings. Defining then the effective statistical segment length b from the relation valid for Gaussian chains, $R_g = b\sqrt{N}/6$, we obtain $b \approx 3.05$. Note that the end-to-end distance is $R \approx 17$, i.e., within our accuracy the relation $R = b\sqrt{N}$ is also fulfilled. Of course, it would be nice to study much longer chains so that the length scales b and R_g are more distinct from each other, but this would require an unreasonable large effort in computer time and thus has not been attempted in the present context.

The Hamiltonian is written in an Ising model type spin representation [42] as

$$\frac{\mathcal{H}}{k_B T} = -\epsilon \sum_{d(i,j) \leq \sqrt{6}} S_i S_j + \epsilon_w \sum_{z_i \leq 2} S_i - \epsilon_w \sum_{z_i \geq D-2} S_i, \quad (1)$$

where $S_i = +1$ if monomer i is of type A, $S_i = -1$ if it is of type B, the interaction parameter ϵ being defined as $k_B T \epsilon = \epsilon_{AA} = \epsilon_{BB} = -\epsilon_{AB}$, if the distance $d(i, j)$ between

monomers does not exceed $\sqrt{6}$, while for more distant neighbors the interaction is zero. From previous work [50] it is known that the critical point of phase separations occurs at $\epsilon_{crit} = 0.0144$, and since we wish to avoid critical fluctuations, we work here at $\epsilon = 0.03$, i.e., far below the critical point ($T/T_{crit} = 0.48$), although experiments are done for [34] $T/T_{crit} \approx 0.95$. In the latter case, however, the correlation length ξ of order parameter fluctuations is already about twice as large as the radius of gyration, while in our case it is distinctly smaller, $\xi \approx 3.6$. Since the correlation length sets the scale for the concentration profile — at least in its wings [9] — one would need to simulate much larger systems for $T/T_{crit} \approx 0.95$ than for the present choice, and in fact with the present computer facilities it is not yet possible to work so close to the critical point. Our choice corresponds to a Flory–Huggins parameter [55, 56] $\chi = 2z_{eff}\epsilon \approx 0.159$ since the effective coordination number is [23] $z_{eff} \approx 2.65$, which is still physically reasonable although it corresponds to a strongly segregated situation ($\chi N \approx 5.09$). From previous work the interfacial tension Σ is known [23] as well; namely $\Sigma/k_B T = \sigma \approx 0.015$.

In Eq.1, a wall interaction of square-well type has been added if monomers are not more distant from the wall than 2 lattice spacings. We choose $\epsilon_w = 0.1$ since from studies of wetting phenomena in polymer mixtures [57] we can safely expect that this choice leads to a wetting transition temperature T_w below the considered temperature. Note that the transition temperature $T_c(D)$ of the interface localization–delocalization transition occurs [31, 32, 33] is expected close to T_w , and we need $T > T_c(D)$ in order to have the situation sketched in Fig.1a (interface delocalized and on average in the middle of the thin film). The absolute magnitude of both surface terms is chosen the same, the sign opposite, so we realize an antisymmetric wall situation, as desired.

The linear dimensions L parallel to the walls are in the range from $L = 64$ to $L = 512$, while $8 \leq D \leq 64$. Remembering that $R_g \approx 7$, our film thicknesses thus range from one R_g to about $9R_g$.

Since these system sizes are rather large, at least for the higher values of D and L , and interfacial fluctuations are notorious slow [32], one must pay much attention to an adequate equilibration of the model system. In the canonical ensemble the order parameter is conserved and we have $\bar{\rho}_A = \bar{\rho}_B$. Two different types of runs have been made: In the first type of runs, “slithering snake” moves [52] (a chain end of a randomly chosen chain is cut at one end and one attempts to join it at the other end in a randomly chosen direction) are mixed with the “random hopping” moves [52, 53] (one tries to move a randomly chosen monomer of a randomly chosen chain in a randomly chosen lattice direction by one unit). It is clear, however, that long range concentration fluctuations will relax rather slowly with this algorithm — diffusion of the chains through the whole system is required. To ease this problem, a second type of runs was tried where the two types of moves mentioned above were combined with chain identity exchanges. To conserve the order parameter, one needs to transform a randomly chosen chain (1) from A to B and another randomly chosen chain (2) from B to A. After some tests we found it useful to mix these moves (slithering snake : random hopping : identity exchange) in the ratios 3:1:0.1 (note that the “1” for the random hopping means one attempted move per monomer of the chosen chain). The total amount of these moves is then counted as “4 Monte–Carlo steps (MCS)” in order to define a “pseudotime” unit for this mixed algorithm. For the semi-grand-canonical ensemble, we always use an algorithm of this

second type, the only distinction being that one attempts an identity change of a single chain (A to B *or* B to A, respectively) instead of an identity exchange between two chains. Since the volume fraction is not conserved, $\bar{\rho}_A = \bar{\rho}_B$ holds on average only, but in general not for individual configurations generated.

Of course, a price one has to pay for these mixing of algorithms is that one performs considerably less moves per second than with algorithms that carry out reptation moves only. E.g., on an IBM RISC 6000-250 workstation one needs only 30 sec to perform 10^6 MCS per chain if only reptation moves are carried out, while the canonical moves including chain exchange take $t \approx 140$ sec, the semi-grand-canonical moves even $t \approx 150$ sec. In order to run a system with $L = 512$ and $D = 32$ for 10^6 MCS for every chain in the system with semi-grand-canonical moves, 700 hours CPU are needed. Since we found it necessary to carry out runs that were partly up to 10 times longer, and many combinations of (L, D) need to be studied, this project is not feasible at workstations as quoted. Fortunately, more powerful machines (including DEC 8400 and SG PowerChallenge) could be accessed.

3 Theoretical background

3.1 Definitions

In this section we define the quantities that will be calculated in the later sections and recall some of the basic theoretical predictions. We denote the coordinate of a point inside two walls as (\mathbf{r}, z) where $\mathbf{r} = (x, y)$ is a two-dimensional coordinate in the surface plane of the left wall (at $z = 0$), and z measures the distance from this wall. From the local densities $\rho_A(\mathbf{r}, z), \rho_B(\mathbf{r}, z)$ of all monomers we define then a local order parameter $m(\mathbf{r}, z)$ as follows:

$$m(\mathbf{r}, z) = \frac{\rho_A(\mathbf{r}, z) - \rho_B(\mathbf{r}, z)}{\rho_A(\mathbf{r}, z) + \rho_B(\mathbf{r}, z)}, \quad (2)$$

while the average order parameter profile is

$$m(z) = L^{-2} \int d\mathbf{r} m(\mathbf{r}, z). \quad (3)$$

Here $\int d\mathbf{r}$ stands symbolically for a summation over the L^2 lattice points in plane z , and $m(z)$ is defined at the discrete points $z = 1, 2, \dots, D - 1$ only, of course.

A quantity of key interest is the order parameter correlation function in the direction parallel to the walls,

$$g(r, z) = \frac{\langle m(\mathbf{r}, z) m(0, z) \rangle - \langle m(0, z) \rangle^2}{\langle m(0, z)^2 \rangle - \langle m(0, z) \rangle^2}, \quad (4)$$

from which we can extract a correlation length $\xi_{||}$ by observing at large distances r an exponential decay,

$$g(r, z = D/2) \propto \frac{1}{\sqrt{r}} \exp\left(-\frac{r}{\xi_{||}}\right). \quad (5)$$

Here we have anticipated (as is also borne out by our numerical data presented below) that the slowest decay of $g(r, z)$ occurs right in the center of the film, due to the interfacial fluctuations [31, 32, 33].

We define the interfacial width w from a fit to a tanh profile,

$$\rho_A(z) = \frac{1}{2} [\rho_{A,coex}^{(1)} + \rho_{A,coex}^{(2)}] + \frac{1}{2} [\rho_{A,coex}^{(2)} - \rho_{A,coex}^{(1)}] \tanh\left(\frac{z - D/2}{w}\right), \quad (6)$$

where the densities of A monomers at the coexistence curve $\rho_{A,coex}^{(1)}, \rho_{A,coex}^{(2)}$ are known from previous work [23, 50]. Alternatively, we can write Eq.6 in terms of $m(z)$ in a more compact form

$$m(z) = m_b \tanh\left(\frac{z - D/2}{w}\right), \quad (7)$$

with $m_b = [\rho_{A,coex}^{(2)} - \rho_{A,coex}^{(1)}] / [\rho_{A,coex}^{(2)} + \rho_{A,coex}^{(1)}]$, noting that for our symmetric mixture $\rho_{B,coex}^{(2)} = \rho_{A,coex}^{(1)}, \rho_{B,coex}^{(1)} = \rho_{A,coex}^{(2)}$. Actually, for our choice of $\epsilon = 0.03$ the mixture in the bulk is essentially fully segregated [23], $\rho_{A,coex}^{(1)} = \rho_{B,coex}^{(2)} \approx 0, \rho_{A,coex}^{(2)} = \rho_{B,coex}^{(1)} \approx \rho_b, m_b \approx 1$, and hence Eq.6 simplifies to

$$\rho_A(z) = \frac{1}{2} \rho_b \left[1 + \tanh\left(\frac{z - D/2}{w}\right) \right]. \quad (8)$$

Since we have chosen to work with only even values for D , the ‘‘Gibbs dividing surface’’ [1, 2] at $z = D/2$ always coincides with a position at the lattice.

The fact that the bulk order parameter $m_b \approx 1$ in our model implies that in the present case the bulk order parameter fluctuations are negligible, and any interplay of bulk and interfacial fluctuations also can be disregarded here. In this sense, the present model is simpler than the Ising model considered in Refs.[32, 33]. (One cannot go to such low temperatures with $m_b \approx 1$ there because the interface roughening transition [58] intervenes.)

3.2 Capillary waves

Our choice of the tanh profile in Eqs.6-8 is motivated by the fact that this form is predicted by mean field type theories, such as Cahn–Hilliard type [6] long wavelength theories [7, 8] and the self-consistent field theory in the limit [13, 14] $\chi N \rightarrow \infty$. All these theories, however, neglect fluctuations in the position of the ‘‘local’’ Gibbs dividing surface which we may define as $[\rho_{A,B}(x, y) = D^{-1} \int dz \rho_{A,B}(x, y, z)]$

$$z_{int}(x, y) = \frac{\rho_A(x, y)}{\rho_A(x, y) + \rho_B(x, y)} D \quad (9)$$

It then is convenient to consider the deviation $h(x, y) = z_{int}(x, y) - D/2$ of this fluctuating interface from its average location. As is well known [1, 2, 3, 4], the idea of capillary wave theory is to put the free energy cost of these fluctuations proportional to the increase in interfacial area caused by these fluctuations. Assuming that the gradients $|\partial h/\partial x|, |\partial h/\partial y|$ are small, this yields (normalizing again by a factor $k_B T$)

$$\Delta F_{CW} = \frac{\sigma}{2} \int dx dy \left[\left(\frac{\partial h}{\partial x}\right)^2 + \left(\frac{\partial h}{\partial y}\right)^2 \right], \quad (10)$$

where it is assumed that σ is simply the bulk interfacial tension (normalized per temperature). By Fourier transformation one obtains from Eq.10 a simple Gaussian Hamiltonian, $h(\mathbf{q})$ denoting the Fourier component of $h(x, y)$ for wavevector \mathbf{q} ,

$$\Delta F_{CW} = \frac{\sigma}{2} \sum_{\mathbf{q}} q^2 |h(\mathbf{q})|^2, \quad (11)$$

and from the equipartition theorem one can immediately conclude that the mean square value of $h(\mathbf{q})$ is [2]

$$\langle |h(\mathbf{q})|^2 \rangle = \frac{1}{\sigma q^2}. \quad (12)$$

This power law spectrum clearly leads to divergences when one computes the local mean square displacement of the interface [1, 2, 3, 4],

$$\begin{aligned} s^2 &\equiv \langle h^2(x, y) \rangle \\ &= \sum_{\mathbf{q}} \langle |h(\mathbf{q})|^2 \rangle \\ &= \frac{1}{4\pi^2} \int d\mathbf{q} \langle |h(\mathbf{q})|^2 \rangle \\ &= \frac{1}{2\pi\sigma} \int dq \frac{1}{q} \\ &= \frac{1}{2\pi\sigma} \ln \left(\frac{q_{max}}{q_{min}} \right) \end{aligned} \quad (13)$$

Since the integral $\int dq/q$ diverges logarithmically both for $q \rightarrow 0$ and $q \rightarrow \infty$, we have heuristically used both a lower cut-off q_{min} and an upper cut-off q_{max} . It is clear that the naive approximation leaving the $1/q^2$ spectrum in Eq.12 completely unmodified in between q_{min} and q_{max} and using these sharp cut-offs needs a closer investigation. It could be necessary to cut off these divergences in a smooth way, using suitable correction terms in the capillary wave Hamiltonian, Eqs.10 and 11, in order to obtain a more accurate description [59]. Even if one accepts Eq.13, the correct choice of q_{min} and q_{max} is a problem, particularly for a polymer mixture. For large enough D such that no confinement effects are felt by these interfacial fluctuations, the minimal value of q possible in the geometries of Fig.1a,b clearly is $q_{min} = 2\pi/L$ (remember that we work with periodic boundary conditions), but the choice of q_{max} is much more questionable: For a small molecule system away from the critical region, one just takes $q_{max} = 2\pi/a$, a being a molecular diameter, while near the critical point $q_{max} = 2\pi/\xi$ as the correlation length ξ then is the only important length scale in the system. For polymer mixtures in the strong segregation limit, we have three length scales to consider: the length scale b of an effective bond, the radius of gyration $R_g = b\sqrt{N/6}$, and the ‘‘intrinsic’’ interfacial width w_0 , which is controlled by the Flory–Huggins parameter χ . According to Helfand’s [13, 14] self-consistent field theory, this intrinsic width is

$$w_0^{SSL} = \frac{b}{\sqrt{6\chi}}. \quad (14)$$

However, the finding of recent computer simulations [23] that the χ parameter itself is not constant in the interfacial region in the strong segregation limit — due to subtle rearrangements in the chain configuration (enhancement of self-contacts, etc.) — has raised doubts on the accuracy of Eq.14, and in fact Eq.14 is not in agreement with the interfacial widths observed in the simulations [22, 23]. Thus, the proper estimation of w_0 may be a problem. Semenov [20] has suggested that w_0 should be used in q_{max} and he concluded

$$q_{max} = \frac{2}{w_0}. \quad (15)$$

Note the absence of a factor π in Eq.15: While in $q_{min} = 2\pi/L$ the constant 2π simply is there due to the periodic boundary condition, there is no condition that actually would fix the constant of proportionality between q_{max} and w_0 !

3.3 Capillary wave broadening of the intrinsic profile: the convolution approximation

The treatment of the previous subsection has implied that the local interface is defined by the coordinate $z_{int}(x, y) = D/2 + h(x, y)$ only, i.e., the interface is considered as a sharp boundary without any intrinsic structure. While this “sharp kink” approximation is reasonable when long wavelength properties are concerned, it clearly does not make sense on small length scales of order w_0 : For length scales L of order $2\pi/q_{max}$ we would have $q_{max}/q_{min} = 1$, i.e., Eq.13 predicts a vanishing mean square interfacial width, which is not a physically sensible result. The standard remedy [4] of this situation is to convolute the intrinsic profile $\rho_A^{(int)}(z)$ (which may be taken of the form of Eq.8 in our case) with a Gaussian distribution of local interface heights,

$$P(h) = \frac{1}{\sqrt{2\pi s^2}} \exp\left(-\frac{h^2}{2s^2}\right), \quad (16)$$

such that the apparent profile becomes

$$\rho_A^{(app)}(z) = \int_{-\infty}^{+\infty} dh \rho_A^{(int)}(z-h) P(h). \quad (17)$$

For explicit calculations it is convenient to replace the tanh function by an error function with the same slope at the midpoint of the profile,

$$\rho_A^{(int)}(z) = \frac{1}{2}\rho_b \left[1 + \tanh\left(\frac{z-D/2}{w_0}\right)\right] \approx \frac{1}{2}\rho_b \left[1 + \operatorname{erf}\left(\frac{\sqrt{\pi}(z-D/2)}{2w_0}\right)\right] \quad (18)$$

We now define the interfacial width w in terms of the maximum slope of the apparent profile,

$$(2w)^{-1} \equiv \frac{1}{\rho_b} \frac{d}{dz} \rho_A^{(app)}(z) \Big|_{z=D/2}. \quad (19)$$

Using Eq.18 in Eq.17 we find

$$w^2 = w_0^2 + \frac{\pi}{2}s^2 \quad (20)$$

and combining this result with Eq.13 yields

$$w^2 = w_0^2 + \frac{1}{4\sigma} \ln \left(\frac{q_{max}}{q_{min}} \right). \quad (21)$$

Eq.21 is the well known result that the mean square broadening due to capillary waves simply has to be added to the square of the intrinsic width.

3.4 Delocalized interfaces in confined geometry

While Secs.3.2,3.3 describe the situation of Fig.1a in the limit $D \rightarrow \infty$ keeping L fixed, we now consider the inverse limit, keeping D fixed but letting $L \rightarrow \infty$. Then the lower cut-off is no longer $2\pi/L$, but rather a correlation length $\xi_{||}$ comes into play [31, 33]. We briefly review the derivation of that length [33]. One again uses a Hamiltonian of the form of Eq.10, but now we need to explicitly consider potentials $V(h)$ exerted by the walls on the fluctuating interface [24, 25, 26, 27, 28, 29, 30, 31, 33]

$$\mathcal{H}_{eff}\{h\} = \int dx dy \left\{ \frac{\sigma}{2} \left[\left(\frac{\partial h}{\partial x} \right)^2 + \left(\frac{\partial h}{\partial y} \right)^2 \right] + V(h) \right\} \quad (22)$$

or more explicitly

$$\begin{aligned} \mathcal{H}_{eff}\{h\} = & \int dx dy \left\{ \frac{\sigma}{2} \left[\left(\frac{\partial h}{\partial x} \right)^2 + \left(\frac{\partial h}{\partial y} \right)^2 \right] \right. \\ & + 2a_0 \left(\frac{T - T_w}{T_w} \right) \exp(-\kappa D/2) \cosh(\kappa h) \\ & \left. + 2b_0 \exp(-\kappa D) \cosh(2\kappa h) \right\} \end{aligned} \quad (23)$$

Note that potentials of the form $\exp(-\kappa D/2) \cosh(\kappa h)$ simply arise from exponentially decaying forces due to the walls

$$\exp[-\kappa z_{int}] + \exp[-\kappa(D - z_{int})] = 2 \exp[-\kappa D/2] \cosh(\kappa h).$$

Here the first potential changes its sign at a temperature T_w to make allowance for the fact that in the semi-infinite system a wetting transition occurs at T_w . The constant κ in mean field theory [31] is identified with the inverse bulk correlation length ξ^{-1} , while more refined treatments imply [31, 60, 61, 62, 63] that κ^{-1} gets renormalized by a factor $(1+\omega/2)$ where ω is the famous parameter entering the theory of critical wetting [26, 64, 65, 66, 67],

$$\kappa^{-1} = \xi(1 + \omega/2), \quad \omega = (4\pi\xi^2\sigma)^{-1} \quad (24)$$

Finally, a_0, b_0 are phenomenological constants that can be calculated from a microscopic theory of interfaces near walls for Ising models [68, 69, 70], but are not known for polymer mixtures, of course.

Also the temperature dependence of the constant ω is known rather accurately for the Ising model [71], but not here. Fig.2 shows a log-log plot of the expected behavior

of ω vs $N(\chi/\chi_{crit} - 1)$. In the mean field critical regime of a polymer mixture (i.e., $|1 - \chi/\chi_{crit}| \ll 1$, but [56, 72, 73] $N|1 - \chi/\chi_{crit}| \gg 1$) one predicts [8, 56] for a lattice model where every site is taken by either an A monomer or a B monomer (i.e., $\rho b^{-3} = 1$),

$$\xi = \frac{b}{6}\sqrt{N} \left(1 - \frac{\chi_{crit}}{\chi}\right)^{-1/2}, \quad \sigma = \frac{8}{3b^2\sqrt{N}} \left(1 - \frac{\chi_{crit}}{\chi}\right)^{3/2} \quad (25)$$

and hence the mean field prediction for ω is [74]

$$\omega_{MF} = \frac{27}{8\pi} \left[N \left(1 - \frac{\chi_{crit}}{\chi}\right) \right]^{-1/2}, \quad N \left|1 - \frac{\chi_{crit}}{\chi}\right| \gg 1. \quad (26)$$

Very close to the critical point (i.e., for $N|1 - \chi/\chi_{crit}| \ll 1$) one expects a crossover to the universal value of the Ising model [71] $\omega_{Ising} = 0.86$. However, more relevant for the present simulations is the behavior of ω in the strong segregation limit. While in the critical regime we have a simple relation between the (intrinsic) width of the interface w_0 and the correlation length [56], $w_0 = 2\xi$, this is no longer true in the strong segregation limit (where $\xi \approx b\sqrt{N}/6$ while w_0 is independent of N , cf. Eq.14). Since ω in the critical region also could be expressed as $\omega = [\pi w_0^2 \sigma]^{-1}$, we suggest that this expression continues to be valid in the strong segregation limit rather than the expression given in Eq.24, cf. Fig.2. Using [13, 14] $\sigma^{SSL} = b^{-2}\sqrt{\chi}/6$ and Eq.14 one obtains

$$\omega_{SSL} = \frac{6}{\pi}\sqrt{6\chi} = \frac{12}{\pi}\sqrt{\frac{3}{N}\frac{\chi}{\chi_{crit}}}, \quad (27)$$

where in the last step the mean field result $\chi_{crit} = 2/N$ was used. Consequently, we assume that also in the equation for κ (Eq.24) one should replace ξ^{-1} by $2/w_0$ in the strong segregation limit.

Expanding $\cosh(\kappa h) \approx 1 + (\kappa h)^2/2$ and omitting constant terms, Eq.23 reduces to

$$\begin{aligned} \mathcal{H}_{eff}\{h\} = & \int dx dy \left\{ \frac{\sigma}{2} \left[\left(\frac{\partial h}{\partial x}\right)^2 + \left(\frac{\partial h}{\partial y}\right)^2 \right] \right. \\ & \left. + \left[a_0 \left(\frac{T - T_w}{T_w}\right) \exp(-\kappa D/2) + 4b_0 \exp(-\kappa D) \right] (\kappa^2 h^2) \right\} \quad (28) \end{aligned}$$

We see that the second term changes sign at [31, 33]

$$T_c(D) = T_w \left[1 - 4 \frac{b_0}{a_0} \exp\left(-\frac{\kappa D}{2}\right) \right], \quad (29)$$

which is the critical temperature of the interface localization–delocalization transition [31, 33]. Of course, even on the mean field level the approximation Eq.28 is only valid for $T > T_c(D)$. In this regime, Eq.28 is formally identical to Ginzburg–Landau theories of second–order phase transitions [1, 2, 3, 4, 56], and thus it is straight forward to obtain the correlation length $\xi_{||}$, using the standard relation

$$\xi_{||}^{-2} = \frac{1}{\sigma} \left(\frac{\partial^2 V(h)}{\partial h^2} \right)_{h=0} \quad (30)$$

to obtain

$$\xi_{\parallel}^{-2} = \frac{2a_0}{\sigma} \kappa^2 \exp\left(-\frac{\kappa D}{2}\right) \left(\frac{T - T_c(D)}{T_w}\right). \quad (31)$$

As expected, ξ_{\parallel} shows a mean field type divergence at $T = T_c(D)$. Even for $T \gg T_c(D)$, however, ξ_{\parallel} is very large for high values of D , due to the factor $\exp(\kappa D/4)$ in the relation $\xi_{\parallel} \approx \kappa^{-1} \sqrt{\sigma T_w / (2a_0 T)} \exp(\kappa D/4)$. If we now assume that it is the length ξ_{\parallel} rather than L that cuts off the capillary wave spectrum, we conclude $q_{min} = 2\pi/\xi_{\parallel}$ and hence Eq.21 becomes

$$w^2 = w_0^2 + \frac{\kappa D}{16\sigma} + const, \quad (32)$$

the constant being $const = (4\sigma)^{-1} \ln \left[\kappa^{-1} q_{max} \sqrt{\sigma T_w / (2a_0 T)} / (2\pi) \right]$. As discussed above, this constant is hard to estimate, and in the simplest approximation it has been neglected [34]. This is justified in the mean field critical region, since $\ln[\dots]$ should be of order unity, and $w_0^2 \gg (4\sigma)^{-1}$ there, but it is not obvious that this approximation is accurate in the strong segregation limit. And again the question must be asked how reliable it is to use ξ_{\parallel} from Eq.31 as a cut-off in a calculation with the “free” capillary wave Hamiltonian, Eq.10, rather than calculating s^2 directly from the full Hamiltonian, Eq.23, without further approximations. Also effects such as a possible position-dependence of the interfacial stiffness (the prefactor of the term $(\partial h / \partial x)^2 + (\partial h / \partial y)^2$) are neglected, although theories have suggested such effects for Ising-like systems [68, 69, 70] Hence a test of Eq.32 by computer simulation is of significant interest.

4 Interfacial profiles, interfacial widths, and the correlation length ξ_{\parallel}

Fig.3 shows some raw data of order parameter profiles in a semi-grand-canonical simulation using $L = 256$ for films of various thicknesses D ranging from $D = 16$ to $D = 64$. The broadening of the profiles with increasing film thickness D is clearly recognized, and qualitatively these data are very similar to earlier results for the Ising model [34]. From a fit of these data to tanh profiles, estimates for the apparent width w as function of L and D is obtained.

In Fig.4, this width w is plotted vs D for $32 \leq L \leq 512$ in the semi-grand-canonical ensemble (sg) and the canonical ensemble with chain exchange (e), respectively. We find three different regimes in our simulations. In the first one, D is small, and the data depend neither on L nor on the type of chosen ensemble. The increase of w^2 with D for $D \leq 16$ even is somewhat stronger than the expected (Eq.32) linear variation. This is due to the fact that for very small D ($D < w_0$) not only capillary wave type fluctuations are suppressed, but even the intrinsic profile gets “squeezed”, and we expect $w \propto D$ (or $w^2 \propto D^2$) as $w \rightarrow 0$; there is just an essentially linear interfacial profile between such walls at extreme proximity of each other. In particular, for $D \rightarrow 0$ the interfacial width w must vanish. Note that additional effects can also be expected due to the squeezing of the chains in quasi-two-dimensional configurations if $D \leq R_g$.

In the second regime for $24 \leq D \leq 56$ and large enough L , data in the semi-grand-canonical ensemble do show the expected variation $w^2 \propto D + \text{const}$. For small L , however, a crossover to the third regime with a steeper rise occurs. This crossover is clearly seen for $L \leq 128$. We expect that for $L = 256$ a similar upturn should occur for $D = 64$, but this is not observed due to the relative large statistical error of this last point (note that the exponential increase of the correlation length ξ_{\parallel} with thickness D , Eq.31, leads to a dramatic slowing down of all Monte–Carlo simulations, and this is responsible for the fact that a small increase of D causes a large increase of statistical errors). This upturn of the curves for large D and relatively small L is interpreted by noticing that we now enter a regime where $L < \xi_{\parallel}$, and then Eq.32 is not valid: In a semi-grand-canonical simulation with periodic boundary conditions the dominating fluctuation is a mode with wavenumber $q = 0$, i.e., a uniform displacement of the interface as a whole ! Thus, there is a finite fraction of the thickness D where the interface can wander back and forth like a rigid straight interface, without feeling much effects of the walls. In the limiting case of $D \rightarrow \infty$ and L small, the interface is freely fluctuating, and thus Eq.19 gives a linear dependence $w = D/2$ [36].

In the canonical ensemble, on the other hand, this third regime is very different. For $L < \xi_{\parallel}$ no significant further increase of w^2 with D occurs; rather w^2 then saturates at a plateau value because in the canonical ensemble a fluctuation of the mean interface position is suppressed, and the capillary wave spectrum now is again limited by L ($q_{\min} = 2\pi/L$) rather than ξ_{\parallel} . Hence, instead of Eq.32 we now have from Eq.21

$$w^2 = w_0^2 + \frac{1}{4\sigma} \ln L + \frac{1}{4\sigma} \ln \left(\frac{q_{\max}}{2\pi} \right) \quad (33)$$

independent of D , which is the standard logarithmic variation of the interface squared width with the lateral linear dimension, as it has often been discussed in the literature [1, 2, 3, 4, 23, 45, 46]. Considering the values of w^2 for $D = 64$ and $L = 32, 64$, and 128 as independent from the finite thickness, we can extract from the slope of w^2 vs $\log L$ the interfacial tension σ and find very good agreement with the simulations of Müller et al [23], i.e., $\sigma = 0.015$.

In order to bring out more clearly these three regimes for the semi-grand-canonical ensemble, we compare in Fig.5a the data for $L = 256$ (which cover the most extensive range of D and are least affected by the finite size effects associated with the smallness of L) with theoretical prediction, Eq.32. As pointed out in Sec.3.4, neither the choices of w_0 nor the choice of κ nor the choice of the additive constant is unique. But the choice made for the parameters in Fig.5a — $\xi = 3.6$ from Monte–Carlo simulations and $w_0 = w_0^{SCF} = 4.65$ as determined in a self-consistent field calculation for our model [22] — is at least plausible, even if the good agreement with the data for $D \geq 40$ is a mere lucky accident. In Fig.5b, a linear plot of w vs D checks for both linear regimes: In the first regime for small D , we find one straight line through the origin, including data where $w \leq w_0$ and using $w(D = 0) = 0$. On the other hand, the crossover to the third regime for large D can be seen whenever ξ_{\parallel} becomes comparable to $L/2$. Since ξ_{\parallel} depends on D as $\xi_{\parallel} \propto \exp(\kappa D/4)$ (Eq.31), it is clear that the location of the onset of the crossover shifts to larger D with increasing L while the first crossover (when w reaches its “intrinsic” value) is independent of L , of course. When L is very small ($L = 32$), the second regime

(where Eq.32 holds) is completely suppressed. For $L \geq 64$, this regime becomes more and more pronounced and an increasing number of data points fall on the expected $L \rightarrow \infty$ curve. Fig.5 illustrates how difficult it is to give interfacial widths observed in simulations a precise meaning.

We now discuss the correlation function $g(r, z)$ (Eq.4), see Figs.6-8. In Fig.6, an example for $L = 256$ and $D = 32$ in the semi-grand-canonical ensemble is shown. It is seen that near walls this quantity has a few oscillations for small r , reflecting the structure of the radial density distribution function, while in the center of the thin film ($z = 16$ in Fig.6) a rather slow decay occurs. This slow decay is the hallmark of the “soft mode phase” described by the theory of Sec.3.4 resulting from interfacial fluctuations. In Figs.7 and 8, the correlation function $g(r) \equiv g(r, z = D/2)$ in the center of the film is studied. A reasonable fit to the expected form of the correlation function (Eq.5) is indeed possible. This is shown in Fig.7 for different film thicknesses ($16 \leq D \leq 48$) using $L = 512$ and the semi-grand-canonical ensemble. The data points (symbols) are fitted to Eq.5 (solid lines), and in this way the correlation length $\xi_{||}$ is determined. However, we must add the caveat that correlation functions of the order of 10^{-3} and distances of the order of $r \geq 40$ are clearly very hard to measure reliably in computer simulations. From Fig.8 it is clear that simulations in the canonical ensemble underestimate $g(r)$ at large r systematically if they are based on local moves and slithering snake moves only. Such observations as shown in Fig.8 have led us to use the present canonical algorithm where also two identity exchanges of chains ($A \rightarrow B$ and $B \rightarrow A$) are attempted as an additional move (data shown by squares in Fig.8). It is also disturbing, however, that there seem to be small systematic differences between the data for the canonical and the semi-grand-canonical ensemble (the estimates for $\xi_{||}$ from Fig.8 are $\xi_{||}(sg) = 22.5$ (circles) and $\xi_{||}(e) = 20.0$ (triangles), even though $L = 256$ exceeds $\xi_{||}$ by about an order of magnitude. Clearly, for $L \rightarrow \infty$ both ensembles should yield identical results for $\xi_{||}$, and in fact for $L = 512$ and $D \leq 40$ this is found (cf. Fig.9). Presumably the observed discrepancy tells that the errors in $\xi_{||}$ (due to statistical errors of $g(r)$) are of order of 10%, or there are unexpectedly large finite size corrections.

Nevertheless it is gratifying that the data for $\xi_{||}$ are compatible with the predicted exponential variation $\xi_{||} \propto \exp(\kappa D/4)$, as shown in Fig.9. The same choice of parameters as assumed in Fig.5a for the interfacial width (Eq.32) gives a good representation of $\xi_{||}$ as function of D . This, in turn, implies that a lot of the ambiguities about the choice of parameters is avoided if we interpret Eqs.21 and 32 in the form $w^2 = w_0^2 + (4\sigma)^{-1} \ln(q_{max}\xi_{||}/2\pi)$ and simply use the measured $\xi_{||}$ in this equation: a straight line with the same slope as included in Fig.5a must result, irrespective of what one assumes for w_0 , q_{max} , κ^{-1} , and ω .

5 A direct test of capillary wave concepts for interfacial fluctuations

The good agreement between the simulation results shown in Figs.4,5,9 and theoretical concepts based on the capillary wave Hamiltonian suggests to study the interfacial fluctuations in more detail. In order to do this, it is convenient to split the system up into columns of block size $B \times B$ and length D and to determine in each column a local

interface position $h(x, y)$ using the concept of the Gibbs dividing surface (in a constant region in the center of the film in order not to be affected by bulk fluctuations). Fig.10 shows snapshot pictures of instantaneous configurations of the interface $h(x, y)$ obtained in this way for a minimal coarse-graining $B = 2$ (columns have the width of the size of one monomer) and the physically more plausible choice $B = 8$ (comparable to the radius of gyration). While for $B = 2$ an extremely rugged “interfacial landscape” results, for $B = 8$ rather pronounced large-amplitude interfacial fluctuations are clearly visible.

Having found $h(x, y)$, we can proceed in the spirit of Sec.3.2 and decompose $h(x, y)$ into Fourier modes $h(q)$, taking into account that possible q -vectors on the lattice are given as $\mathbf{q} = (q_x, q_y) = 2\pi/L (i, j)$ with i, j integers. For simplicity, we consider only a wavevector in a lattice direction, and hence classify the $h(\mathbf{q})$ as h_i . Since Eq.12 implies $\langle |h_i|^2 \rangle = (\sigma q_i^2)^{-1} \propto i^{-2}$, we present a log–log plot of $\langle |h_i|^2 \rangle$ vs i^{-2} in Fig.11. Pure capillary waves in this representation should show up as straight lines with a slope of unity. For $L = 256$ and $D = 56$ and 64 , this is indeed found for $2 \leq i (< 20)$, but even for this largest studied thicknesses we still see deviations due to finite D for $i = 1$! For $D \leq 48$, this effect becomes more important and modes $i = 2, 3, \dots$ are affected by the finite thickness D . One could suspect that there is a problem of equilibration of the largest length scales of interfacial fluctuations, but this is not a problem here as an analysis of the autocorrelation function $C_{hh}(t) = [\langle h_i(t)h_i(0) \rangle - \langle h_i \rangle^2] / [\langle h_i^2 \rangle - \langle h_i \rangle^2]$ of the modes as a function of time measured in Monte–Carlo steps (MCS) shows (Fig.12). The relaxation times of these fluctuations ($\tau = \mathcal{O}(10^4 \text{MCS})$) are much smaller than the simulation runs ($\tau = \mathcal{O}(10^6 \text{MCS})$).

An alternative analysis is to vary the block size B over a wide range and estimate the mean square width w^2 as a function of block size. This is shown in Fig.13 for $L = 128$. Here the interfacial position h is determined in all columns. The monomer profile is taken relative to this position, $\rho_A(z - h)$, and after averaging over all columns in the system, the interfacial width is determined by a fit to a tanh profile. For $D = 56$ and 64 , one sees a constant slope for $B \geq 8$, as expected for capillary waves independent of film thickness D . Note that the largest block size $B = 128$ is different from the smaller ones. For $B = L$ periodic boundary conditions apply. Thus, the capillary wave spectrum is cut off by $q_{min} = 2\pi/L$. In contrast, for $B < L$ the boundary conditions are free (as in experimental situations) and a supplementary mode appears characterized by $q = \pi/B$. For $D = 16$, there is an upper cut-off block size which gives a w independent of B , but typical for $D = 16$. For $24 \leq D \leq 48$, we find a rather slow crossover from a D -dominated to a L -dominated interfacial width for the largest block size. On the other hand, the curves differ as well for all the small block sizes in function of the film thickness D , and this difference is almost constant for $4 \leq B \leq 32$. This is a sign that there are two contributions to the variation of the interfacial width with B and D : The first arises from capillary waves; it depends on the block size B , and the finite thickness D acts as a new cut-off length scale $\xi_{||}$. On the other hand, there is a second contribution that depends on D only, not on B . It can thus be attributed to a change in the “intrinsic width” of the interface due to the presence of the walls.

For very small block sizes, w^2 becomes flat, and from this crossover one hence might attempt to estimate both w_0 and q_{max} directly. This would yield $w_0 \approx 3$ and $q_{max} \approx 2\pi/5$ for $D = 24$, and $w_0 \approx 4$ and $q_{max} \approx 2\pi/6$ for $D = 64$. But exact values are hard to

give since there is a no sharp cut-off, but rather a smooth crossover. The three important length scales monomer size, correlation length ξ , and width w being close to each other, this analysis does not really clarify the questions concerning the cut-offs.

Nevertheless the change of the intrinsic width with D extracted from Fig.13 can be included quantitatively in our capillary wave analysis. For this purpose, we define $w(D, B = 8) = w_0(D)$ as the intrinsic width of our system. With this choice we are on the safe side, i.e. the further variation of $w(D, B)$ in function of B can be described in terms of a capillary wave broadening. For $B < 8$, Fig.13 indicates the onset of the crossover to a saturation value of w_0 . We take then the data from Fig.5b for $w^2(D)$ and in Fig.14 $w_c^2(D) = w^2(D) - w_0^2(D)$ is plotted. In that way, a constant slope of w_c^2 vs D is obtained over the whole range of simulations as required by Eq.32. The straight line shows the theoretical prediction with the same choice of parameter as before. The main result is that both slopes agree very well. Since in our case $w_0^{SCF} \approx w_0^{sim}(D \rightarrow \infty, B = 8)$, even the absolute values are the same (w_0^{sim} denotes the interfacial width extracted from simulations). Of course, from our data one could as well define $w(D, B = 4)$ as intrinsic width. Then we would recover the theoretical result by choosing a constant term in Eq.32 larger than zero.

Finally Fig.15 considers the distribution of interface locations $P(h)$. It is seen that Gaussian distributions give a very good fit to such data. Using $w^2(D, L = 128) = w_0^2(D) + (\pi/2)s^2(D)$ and $w^2(B = 8)$ from Fig.13, we find $w^2(D = 24, L = 128) = 15.1 + (\pi/2) 3.54^2 = 34.8$ and $w^2(D = 64, L = 128) = 21.8 + (\pi/2) 4.67^2 = 56.1$, in good agreement with the direct results in Fig.13. This shows once more the self-consistency of our analysis.

6 Conclusion

In this paper we have studied the size-dependence of interfacial profiles between coexisting phases of mixtures confined between parallel walls, considering both the dependences on the linear dimension L parallel to the interface and the perpendicular linear dimension D . The temperature of the system is above the wetting temperature T_w , and the interface is delocalized and on average in the center of the film. We argue that in this regime the interfacial correlation length $\xi_{||} \propto \exp(\kappa D/4)$, proposed first by Parry and Evans [31] assuming that κ^{-1} is the correlation length ξ of concentration fluctuations in the bulk, acts like a cut-off for the capillary wave spectrum, $q_{min} = 2\pi/\xi_{||}$. Using the convolution of capillary wave broadening with the ‘‘intrinsic’’ profile of width w_0 , we propose in the limit $L \gg \xi_{||}$ the formula for the total interfacial squared width $w^2 = w_0^2 + (4\sigma)^{-1} \ln(q_{max}/q_{min}) \approx w_0^2 + (16\sigma)^{-1} \kappa D$, where σ is the interfacial tension. This phenomenological approach is tested by a Monte-Carlo simulation of a model for a symmetrical polymer mixture in the strong segregation limit, and reasonable agreement is found, although the precise choice of parameters (cut-off q_{max} , length κ^{-1} , capillary parameter ω in the relation $\kappa^{-1} = \xi(1 + \omega/2)$ proposed by recent theories [60, 61, 62, 63]) may need refinement.

Of course, the above formula is only an asymptotic result for $D \gg w_0$; for smaller values of D we find a regime where capillary wave type excitations are not yet important,

and rather the intrinsic profile itself is “squeezed down” by the confinement. In this region $w \propto D$ (with a prefactor considerably smaller than unity) until w has reached roughly the value w_0 of the intrinsic interface without confinement. Note that there $D/2$ is comparable to the largest eigenvalue of the gyration tensor of the chains, and hence an effect on the chain configuration due to the confinement is already expected. This effect will be studied more closely in future work.

The limit $\xi_{||} > L$ deserves attention, too. We find that the above behavior $w^2 \approx w_0^2 + (16\sigma)^{-1}\kappa D$ only holds until about $\xi_{||} = L/2$, and then a regime sets in which depends on the type of ensemble used: In the canonical ensemble, the average position of the interface is fixed at the middle of the system, and the capillary wave spectrum is cut off by $q_{min} = 2\pi/L$ rather than $q_{min} = 2\pi/\xi_{||}$. As a result, $w^2 = w_0^2 + (4\sigma)^{-1} \ln(q_{max}L/2\pi)$ in this regime, independent of D . In the semi-grand-canonical ensemble, on the other hand, there is also a fluctuation described by a wavenumber $q = 0$, i.e., a uniform mode in which the interface fluctuates back and forth as a whole without bending. This leads to a behavior $w \propto D$ for $D \rightarrow \infty$.

As a result, the meaning of interfacial profiles and interfacial widths is rather delicate. This is not only a problem of computer simulations — it is encouraging to note that the analysis presented here is immediately useful for the interpretation of corresponding experiments [34, 47]. Of course, in experiments it may be sometimes necessary to work with long range surface forces (inverse power law decay) rather than the exponential decay assumed here. It is obvious that this will reduce the exponential growth of $\xi_{||}$ with D into a power law growth as well, and since $\ln \xi_{||} = \ln D^p = p \ln D$ for any power p , we obtain a behavior $w^2 \propto \ln D$ rather than $w^2 \propto D$, as found here. A detailed analysis of this situation is still lacking.

Many of our findings carry over to the other simulation geometries considered in Fig.1, such as antiperiodic boundary conditions or fully periodic boundary conditions. Note that in the latter case only the canonical ensemble is useful because otherwise the situation with two interfaces is unstable. In the antiperiodic case both ensembles may be used, but since one translates the interface to the center of the system by construction, the “uniform mode” leading to the above behavior $w^2 \propto D^2$ is absent, and the finite size effects in the canonical and semi-grand-canonical ensembles are very similar then. We do hope that the present analysis will stimulate a careful assessment of these finite size effects in future simulations of interfacial properties since we feel that much previous work has been hampered by inadequate interpretation of fluctuation–broadened interfacial profiles as “intrinsic profiles”. The present work indicates that a unique characterization of “intrinsic profiles” encounters difficulties even if size effects are carefully taken care of.

Acknowledgements

Support by the Deutsche Forschungsgemeinschaft (DFG), grant No.Bi-314/3-4, and by the Bundesministerium für Bildung, Wissenschaft, Forschung und Technologie (BMBF), grant No.03N8008C, is gratefully acknowledged. We thank J.Klein and T.Kerle for stimulating discussions. We acknowledge access to the computer facilities of the ZDV, University of Mainz, and the RHR Kaiserslautern.

Figure captions

Fig.1: Typical geometries used in computer simulations (a,b) and in experiment (c) in order to study interfacial profiles. Only one lateral direction parallel to the average interface plane is shown. The schematic plots indicate “coarse-grained snapshots” of the system, i.e., bulk fluctuations in both the A-rich phase and the B-rich phase are averaged out, and the resolution perpendicular to the interface does not resolve the “intrinsic” interfacial profile in these pictures. Case (a) shows geometries where a single interface occurs [23, 32, 33, 34, 39], while case (b) refers to a situation with two (on average parallel) interfaces confining a slab like region of B-rich phase in between [40]. While the left case of (a) has the disadvantage that perturbations due to the two hard walls must affect the interfacial profile if D is not large enough, the right case of (a) is only possible for strictly symmetric mixtures (“antiperiodic boundary conditions” means that an A-particle that leaves the simulation box on the right side reenters as a B-particle on the left side, while no identity switches of particles occur across periodic boundaries). In case (c) it is assumed that the direction of gravity is from left to right and that the B-rich phase is favored by the air while the A-rich phase is favored by the right wall (walls of the container at the bottom and at the top are assumed to be neutral). Note that here linear dimensions are not to scale (e.g. the sample lateral dimension L_{sample} may be macroscopically large and exceed the lateral resolution length scale L by several orders of magnitude), and also the fluctuations of the coarse-grained interface are simplified (short wavelengths being omitted, amplitudes of long wavelengths exaggerated for clarity).

Fig.2: Log-log plot of ω vs $\chi/\chi_{crit} - 1$, for chain lengths ranging from $N = 128$ to $N = 1024$, showing the predictions for ω_{Ising} , ω_{MF} (Eq.26), and ω_{SSL} (Eq.27) using $\rho b^3 = 1$.

Fig.3: Order parameter profile $m(z)$ vs $z - D/2$ for films of thicknesses $D = 16, 32, 48$, and 64 , as indicated by different symbols. The interface is centered at the origin $z = D/2$, walls being situated at $z = 0$ and $z = D$. All data refer to a lateral system size of $L = 256$ and the semi-grand-canonical ensemble. The lines through the data points are fits to $m(z) = m_b \tanh [(z - D/2)/w]$. Note that statistical errors are smaller than the size of the symbols.

Fig.4: Plot of the square of the apparent interfacial width w^2 vs film thickness D for several choices of L ($L = 32, 64, 128, 256$, and 512) and two choices of statistical ensembles: the canonical ensemble including identity exchanges (opaque symbols marked by (e)) and the semi-grand-canonical ensemble (filled symbols marked by (sg)). Note that the accuracy of these data is very good for small D , while for the two largest values of D ($D = 56, 64$) statistical errors are estimated to exceed the size of the symbols several times. For $L = 512$, values of w^2 are determined up to $D = 48$ and, within statistical error, no difference between the ensembles is found and, thus, points in Fig.4 lie on top of each other.

Fig.5: a) Squared interfacial width w^2 vs film thickness D for $L = 256$ in the semi-grand-canonical ensemble. The straight line shows Eq.32, neglecting the last term on the

right hand size and using $\kappa^{-1} = \xi(1 + \omega/2)$, $\xi = 3.6$, $\omega^{-1} = 4\pi\xi^2\sigma$, $\sigma = 0.015$, and $w_0 = w_0^{SCF} = 4.65$ [22].

b) Interfacial width w plotted vs D for $L = 32, 64, 128$, and $L = 256$ using the data from the semi-grand-canonical ensemble simulations. For small D , one has a linear variation $w \propto D$ up to $w \approx w_0$ (squeezed intrinsic interface). Arrows show that the regime of free interface fluctuation sets in for $\xi_{||} = L/2$. The dashed line is the limiting case of completely free fluctuations of the interface, i.e., $w = D/2$. Also the self-consistent field estimate for the intrinsic interfacial width (w_0^{SCF}) is shown. Data for $\xi_{||}$ have been taken from Fig.9 below.

Fig.6: Correlation function $g(r, z)$ (Eq.4) plotted as function of both variables $r = \sqrt{x^2 + y^2}$ and z for the case $L = 256$, $D = 32$.

Fig.7: Semilog plot of correlation functions $g(r) \equiv g(r, z = D/2)$ in the center of the thin film vs r for $L = 512$ and general choices of D as indicated. All data refer to the semi-grand-canonical ensemble. Curves are fits to $g(r)$ to the form $g(r) \propto r^{-1/2} \exp(-r/\xi_{||})$, cf. Eq.5.

Fig.8: Semilog plot of correlation functions $g(r)$ vs r for $L = 256$ and $D = 32$ for different ensembles: semi-grand-canonical ensemble (circles), canonical ensemble (triangles) including chain identity exchanges, while squares indicate results with local moves and slithering snake moves only. Curves are fits to Eq.5.

Fig.9: Correlation length $\xi_{||}$ plotted vs D obtained by a fit of $g(r)$ to Eq.5 for $L = 512$ and film thicknesses $D \leq 48$ using both data for the canonical ensemble (triangles) and the semi-grand-canonical ensemble (circles). Within statistical errors, both ensembles yield identical results for $D \leq 40$, but differ for $D = 48$. Full curve is the formula $\xi_{||} = \xi \exp(\kappa D/4)$, using $\kappa^{-1} = \xi(1 + \omega/2)$ and $\xi = 3.6$ as obtained from an independent simulation.

Fig.10: Typical plot of a snapshot picture of the local interface positions $h(x, y)$ for $D = 64$, $L = 64$ using the minimal coarse-graining (i.e., block size $B = 2$) in case (a) and modest coarse-graining ($B = 8 \approx R_g$) in case (b).

Fig.11: Log-log plot of the mean square Fourier component $\langle |h_i|^2 \rangle$ of the interfacial fluctuations vs i^{-2} for $L = 256$ and the canonical ensemble. Several choices of D are included as indicated in the figure. The straight line shows the theoretical prediction from the capillary wave Hamiltonian, i.e., $\langle |h_i|^2 \rangle = (\sigma q^2)^{-1} = [L/(2\pi i)]^2 \sigma^{-1}$.

Fig.12: Semilog plot of the autocorrelation function $C_{hh}(t) \equiv [\langle h_i(t)h_i(0) \rangle - \langle h_i \rangle^2] / [\langle h_i^2 \rangle - \langle h_i \rangle^2]$ vs time t (in Monte-Carlo steps MCS). Data refer to $L = 256$, $D = 48$ using the canonical ensemble with chain identity exchanges. The two slowest modes ($i = 1, 2$) are shown. Lines are fits of $-\ln[C_{hh}(t)]$ to an exponential decay. Even for the slowest mode ($i = 1$) the autocorrelation time $\tau \approx 1.5 \cdot 10^4$ MCS is much smaller than the time of typical simulation runs.

Fig.13: Plot of the squared interfacial width w^2 vs the block size B (note the logarithmic scale) for a system of lateral linear dimension $L = 128$ and thicknesses D as indicated.

Fig.14: Same data as presented in Fig.5a ($L = 256$, semi-grand-canonical ensemble), but only the contribution $w_c^2(D) = w^2(D) - w_0^2(D)$ due to capillary waves is shown. The intrinsic width $w_0(D)$ is taken from Fig.13 ($L = 128$, canonical ensemble) as the width determined in blocks of $B = 8 \approx R_g$. The straight line is the broadening according to theory (cf. Eq.32), i.e., $w_c^2 = \kappa D / (16\sigma)$.

Fig.15: Distribution of interface locations $P(h)$ for $L = 128$, $24 \leq D \leq 64$ using a coarse-graining size $B = 8$. Lines are fits to the theoretical assumption of a Gaussian distribution $P(h) = (2\pi s^2)^{-1/2} \exp[-h^2/(2s^2)]$. The values of s obtained by this fit are indicated.

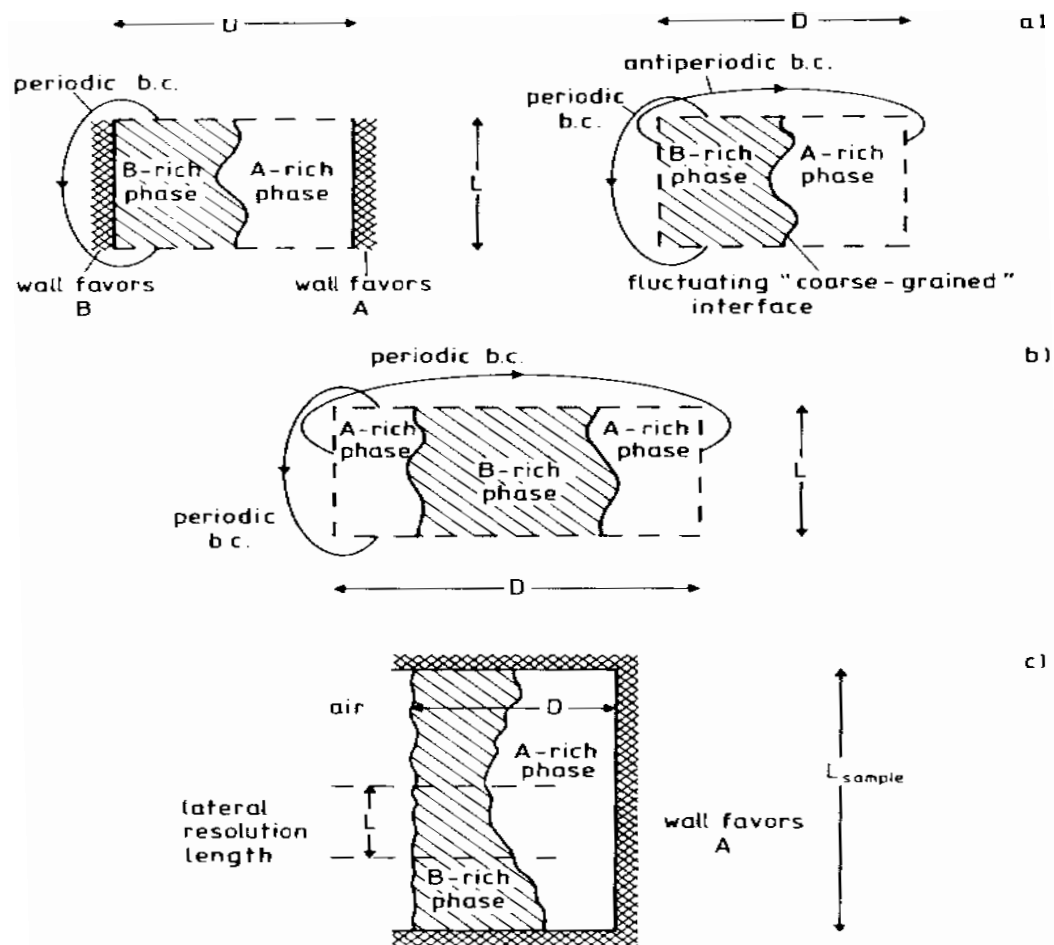


Fig 1

Figure 1
Werner et al
JCP

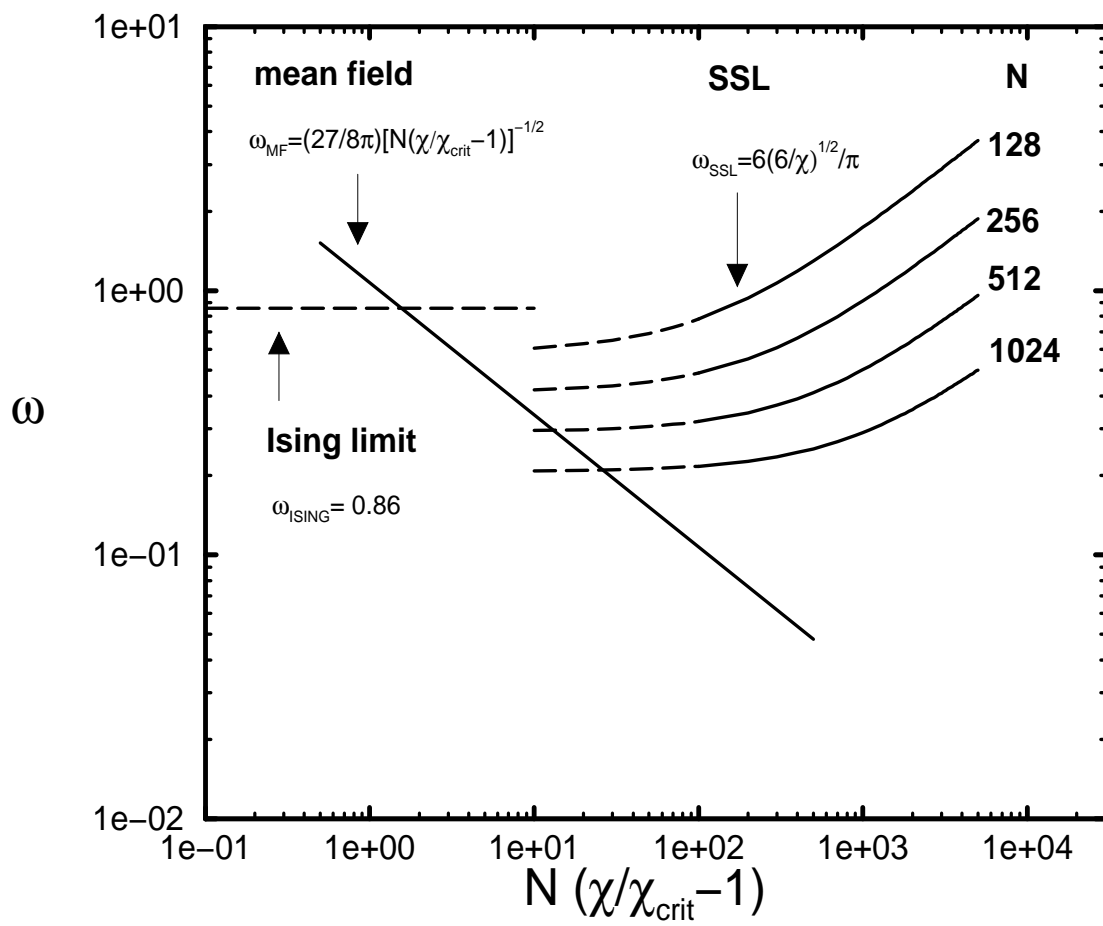


Figure 2
 Werner et al
 JCP

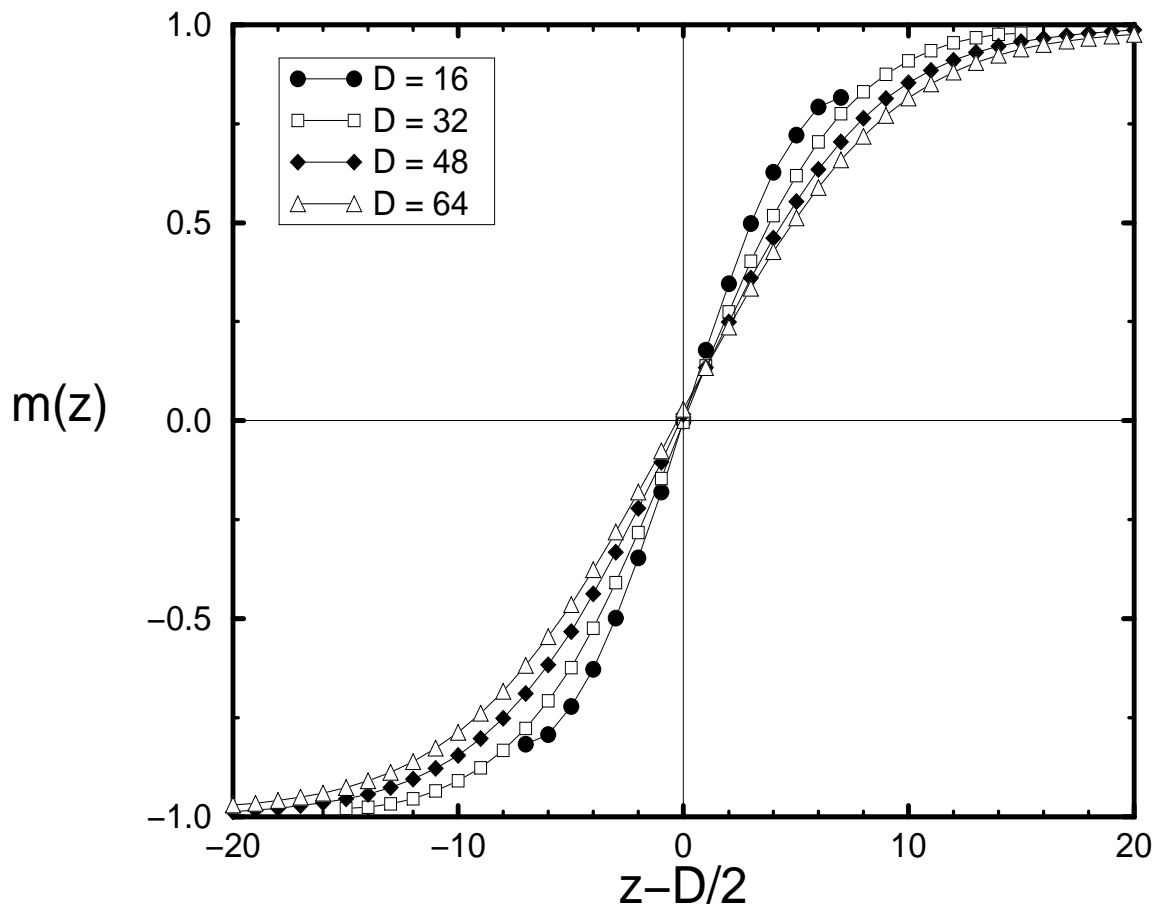


Figure 3
Werner et al
JCP

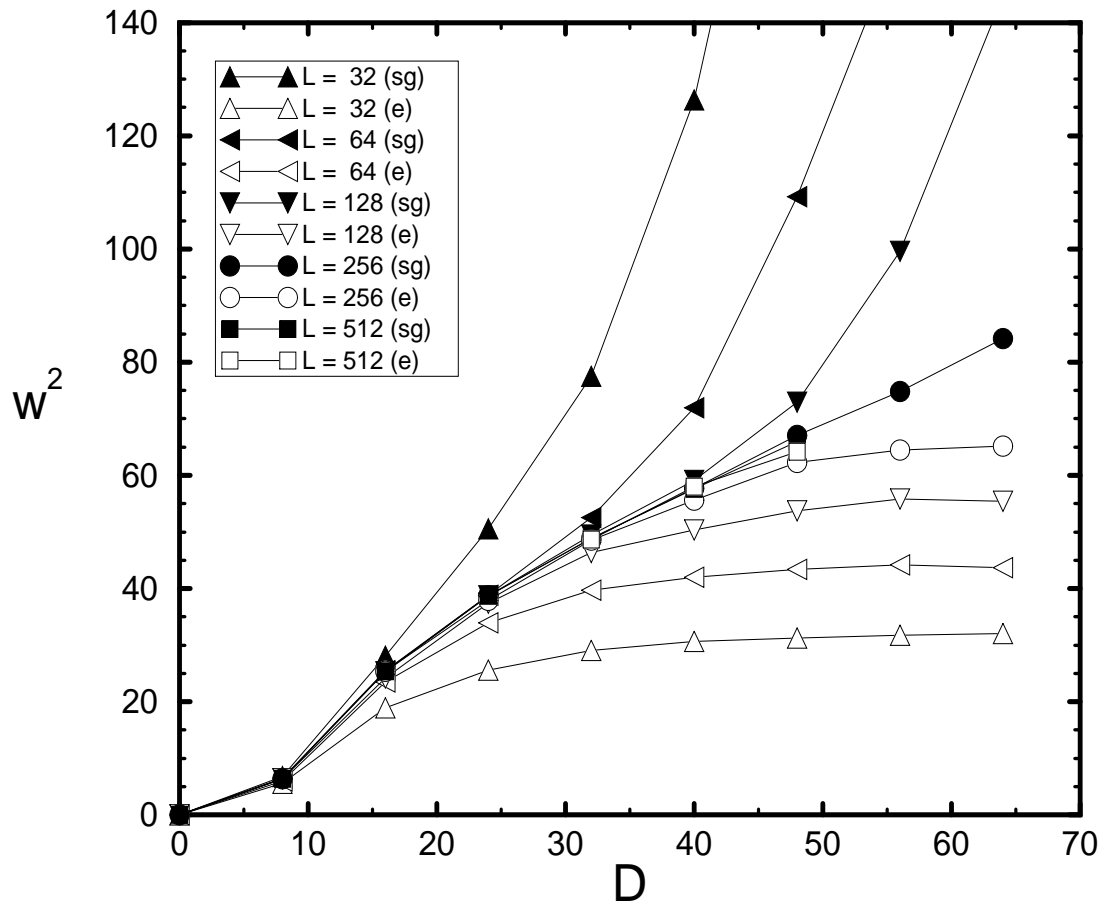


Figure 4
Werner et al
JCP

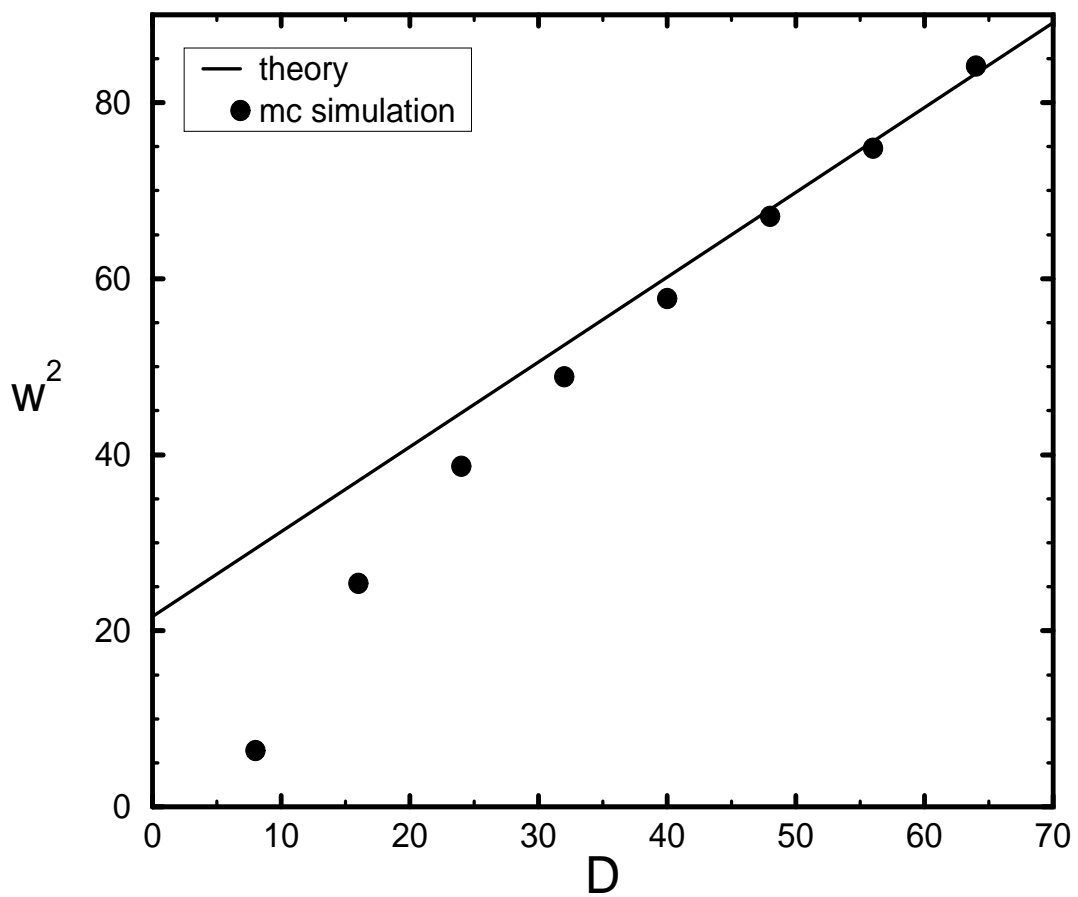


Figure 5a
Werner et al
JCP

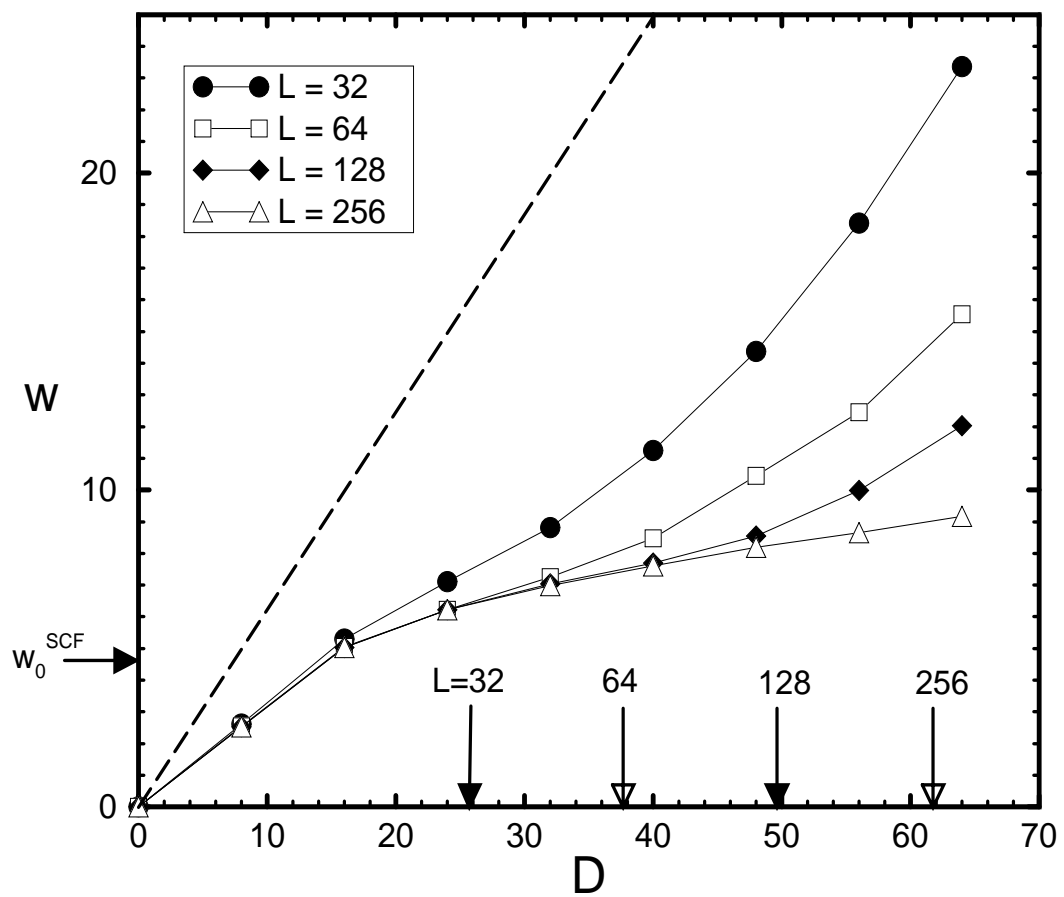


Figure 5b
 Werner et al
 JCP

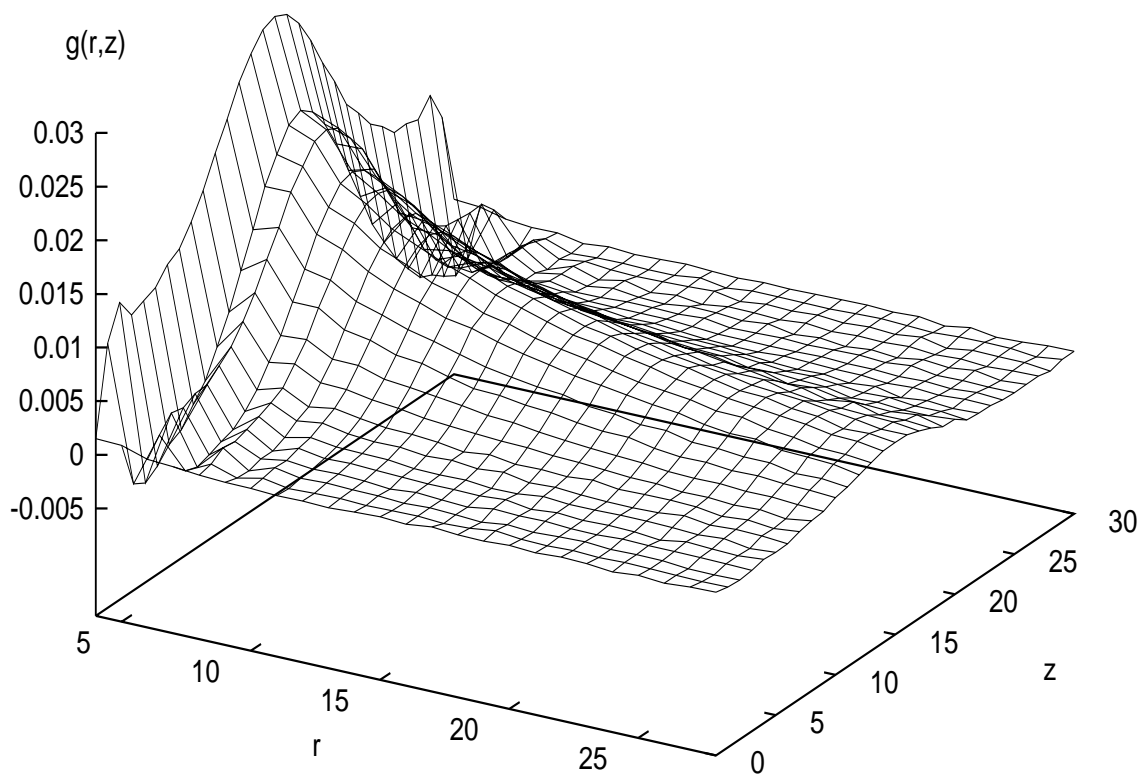


Figure 6
Werner et al
JCP

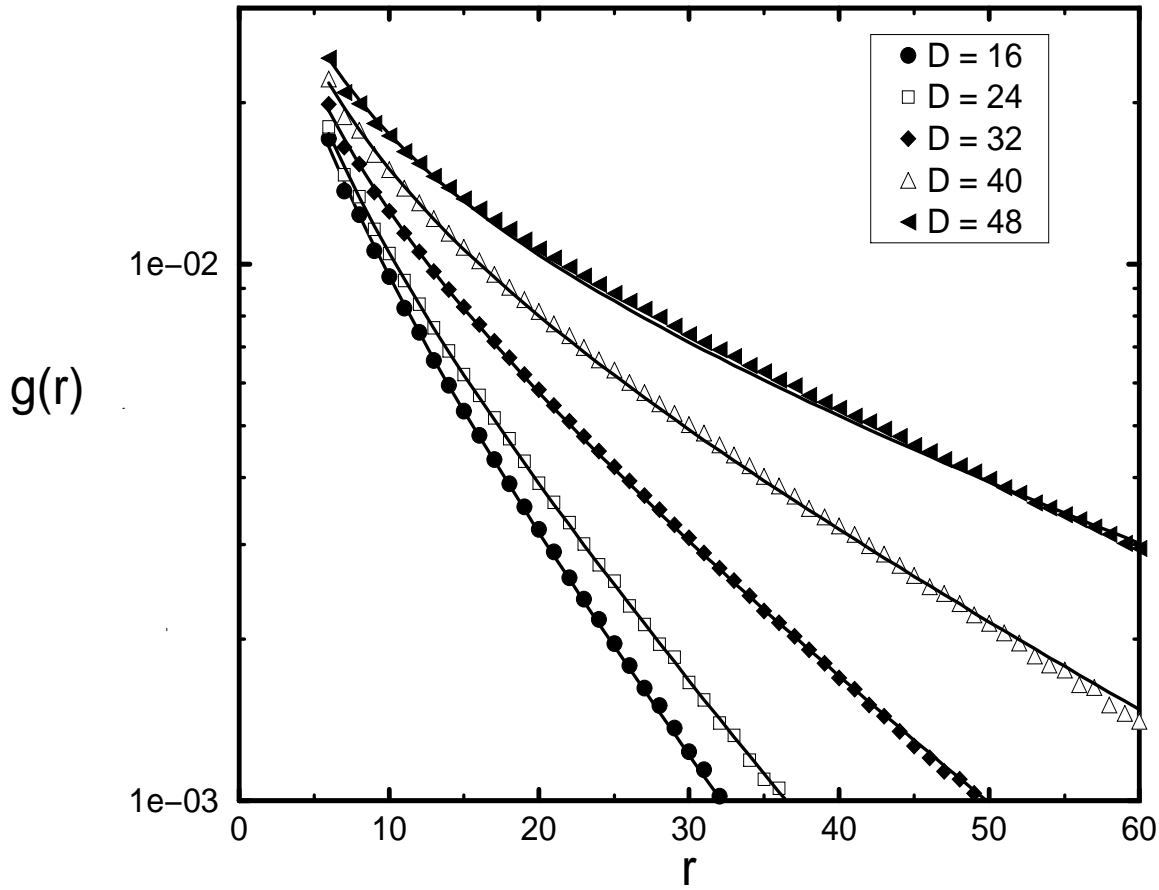


Figure 7
Werner et al
JCP

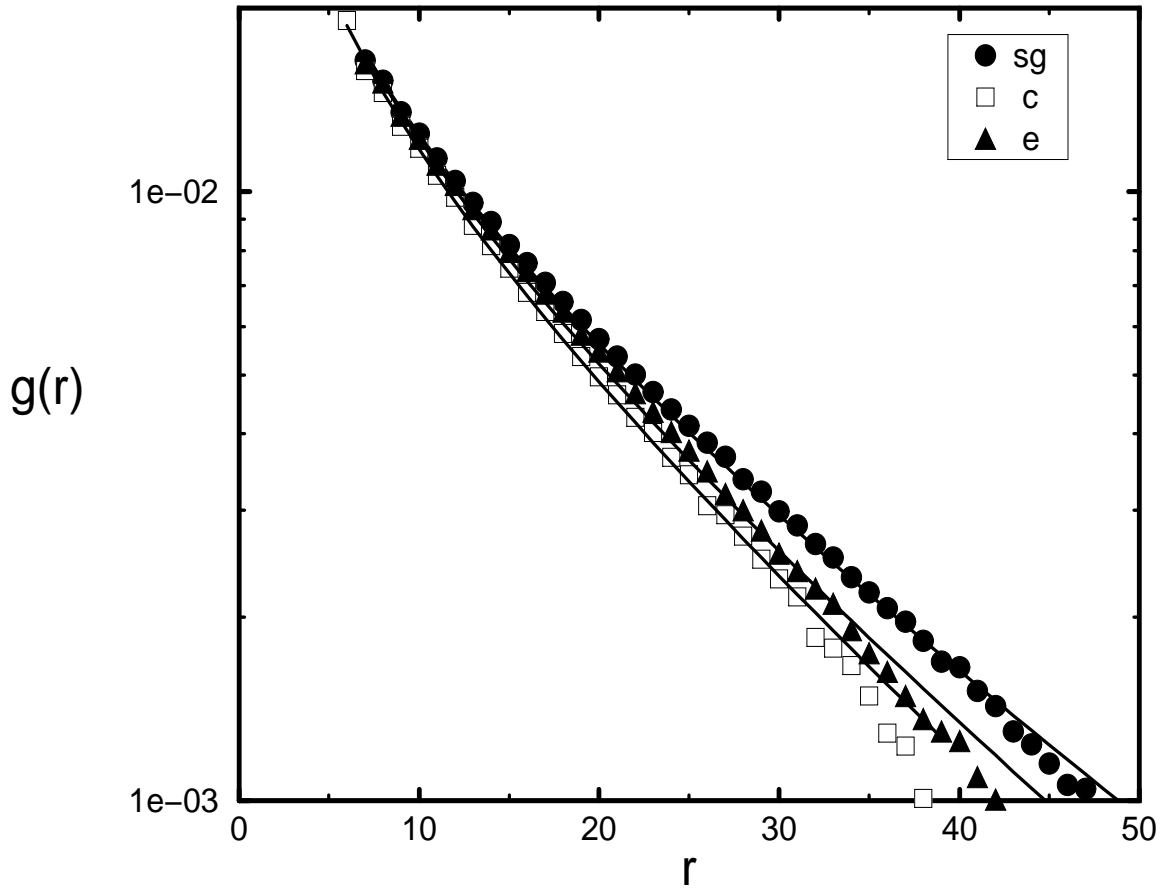


Figure 8
Werner et al
JCP

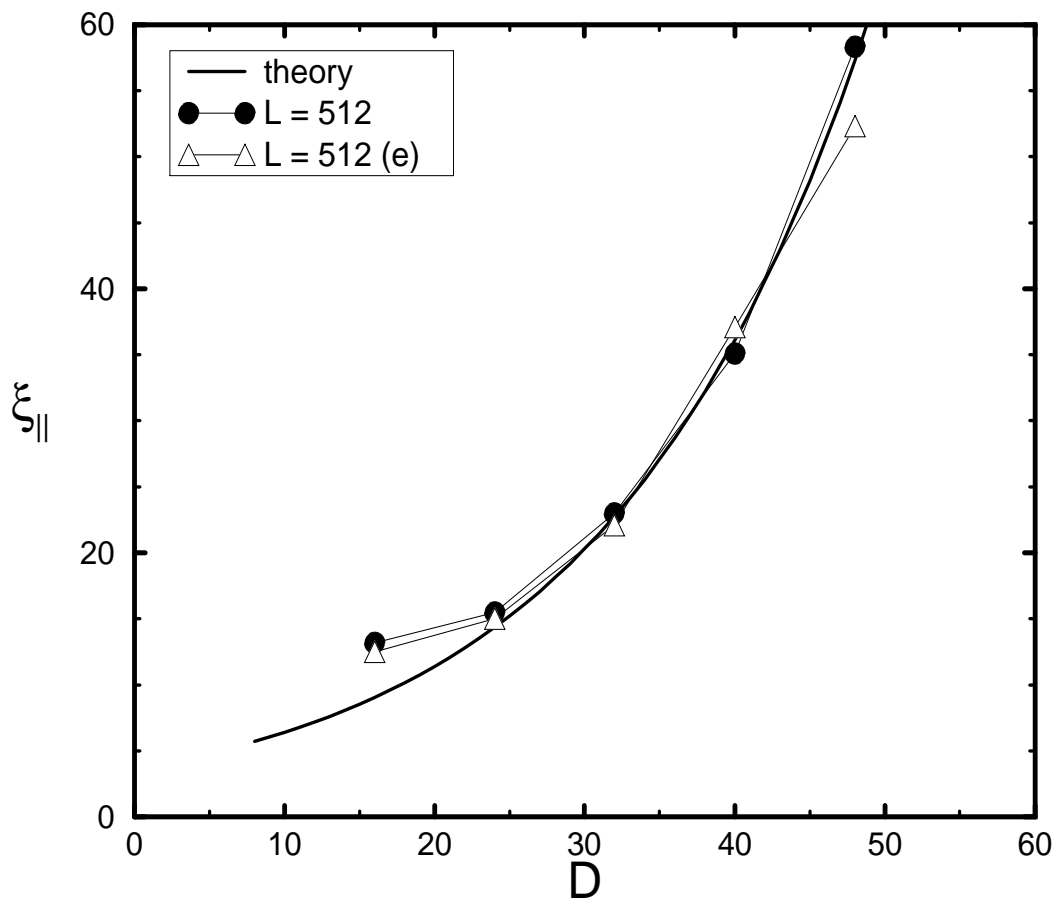


Figure 9
Werner et al
JCP

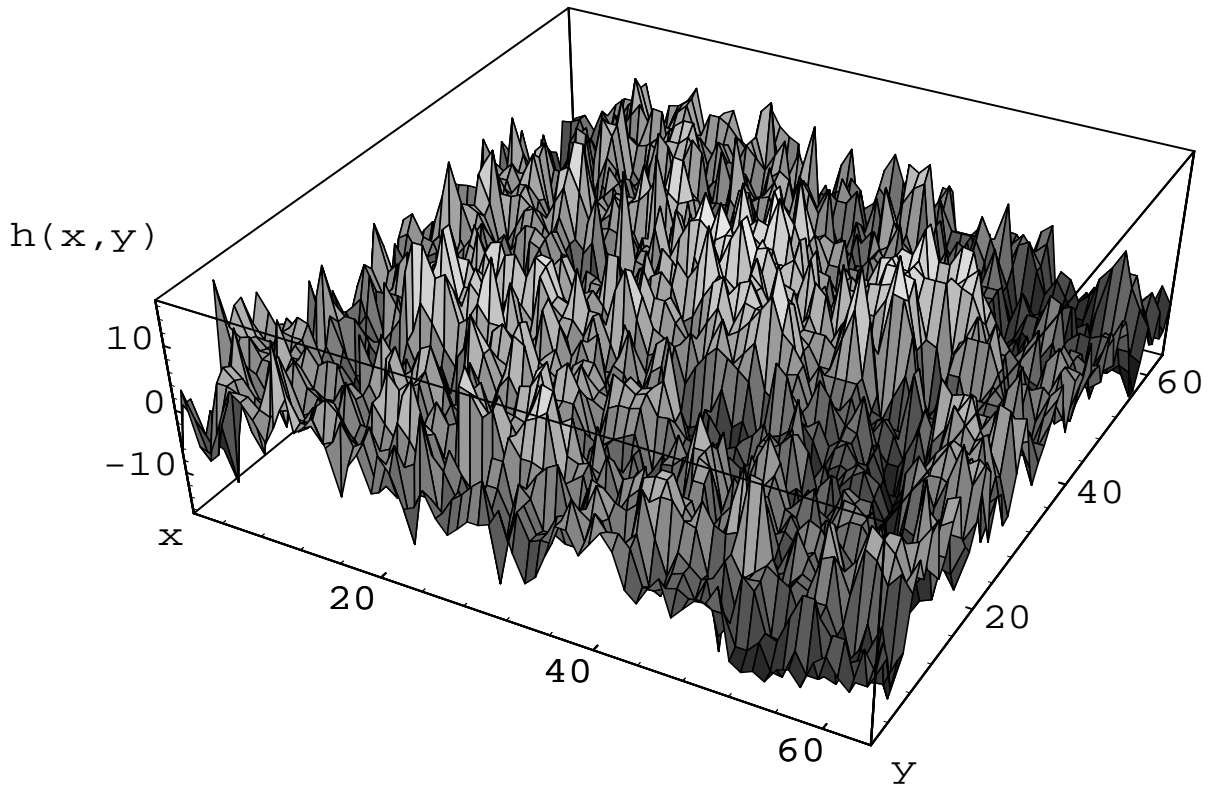


Figure 10a
Werner et al
JCP

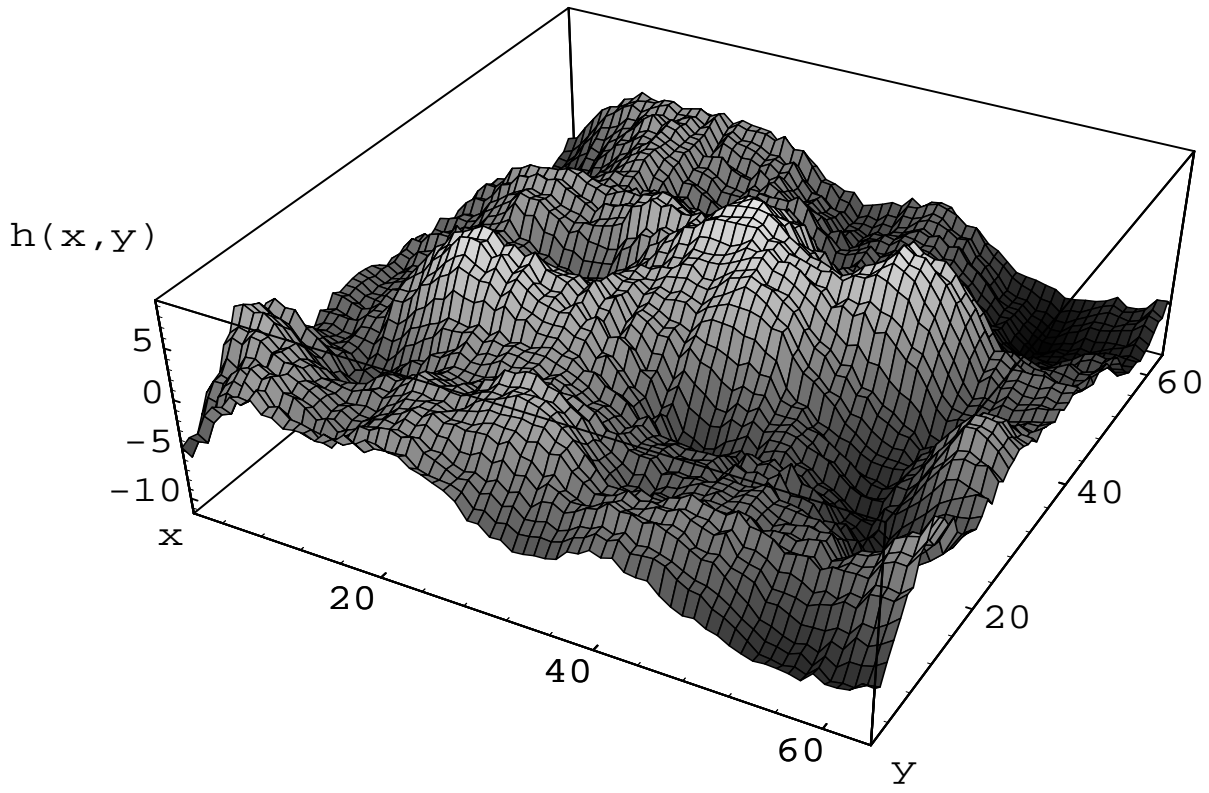


Figure 10b
Werner et al
JCP

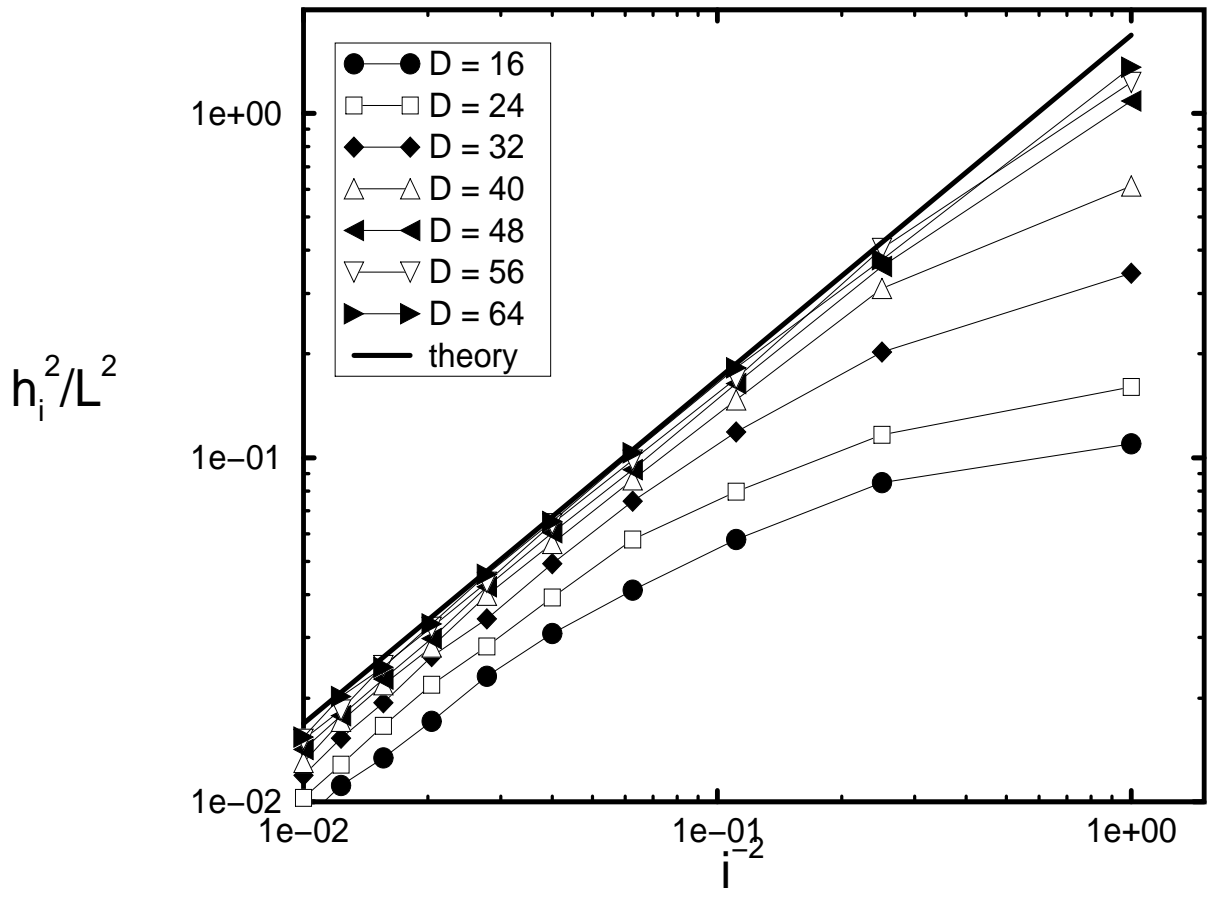


Figure 11
Werner et al
JCP

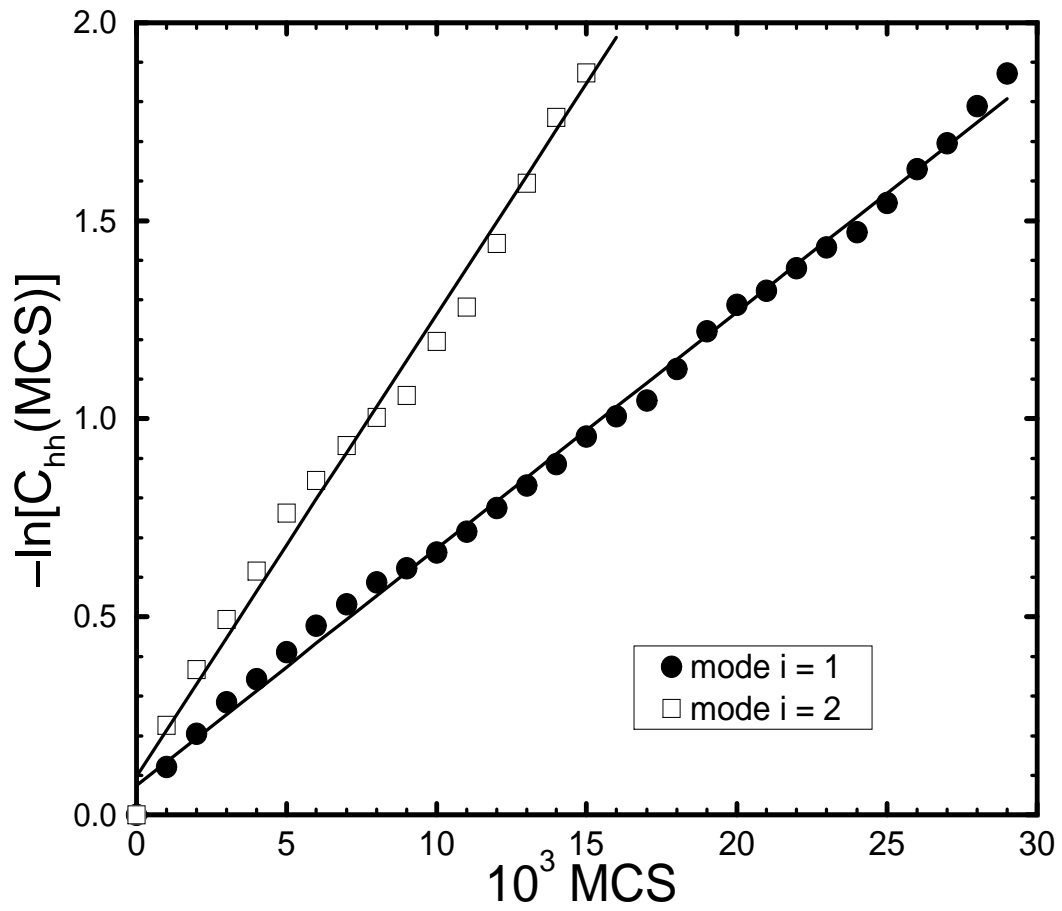


Figure 12
Werner et al
JCP

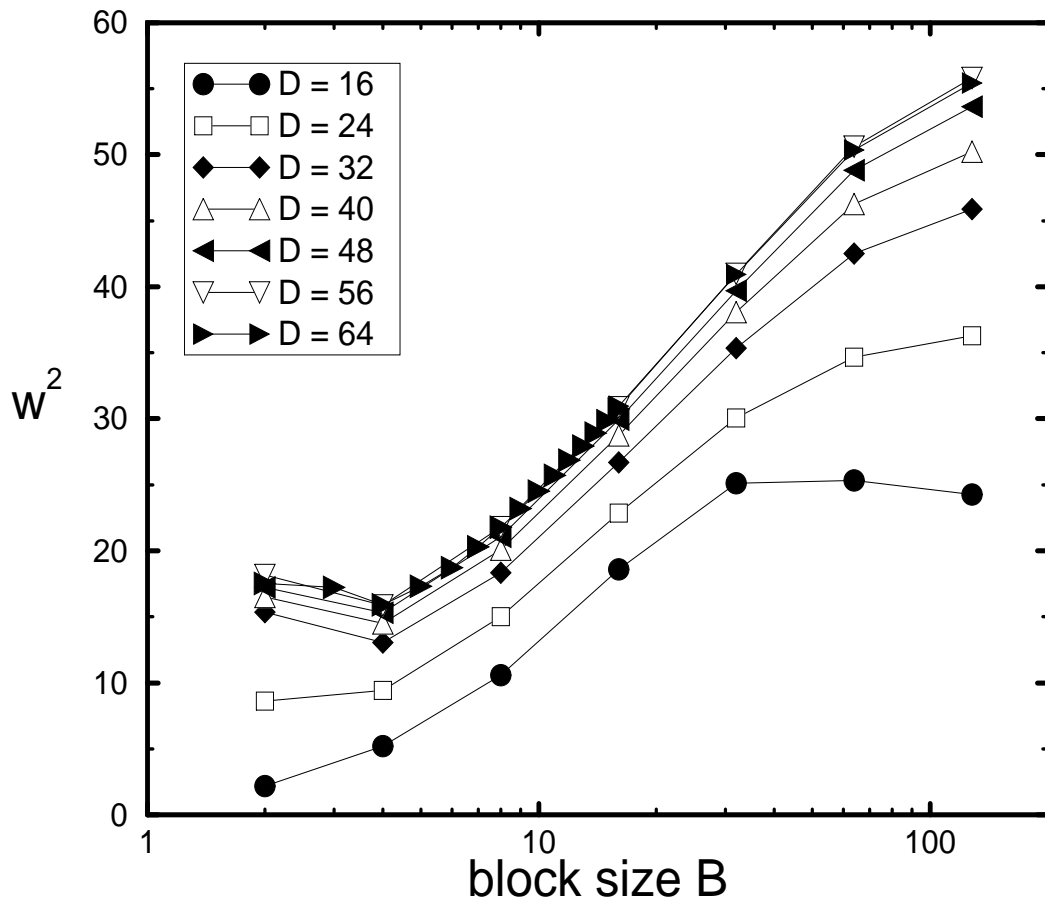


Figure 13
 Werner et al
 JCP

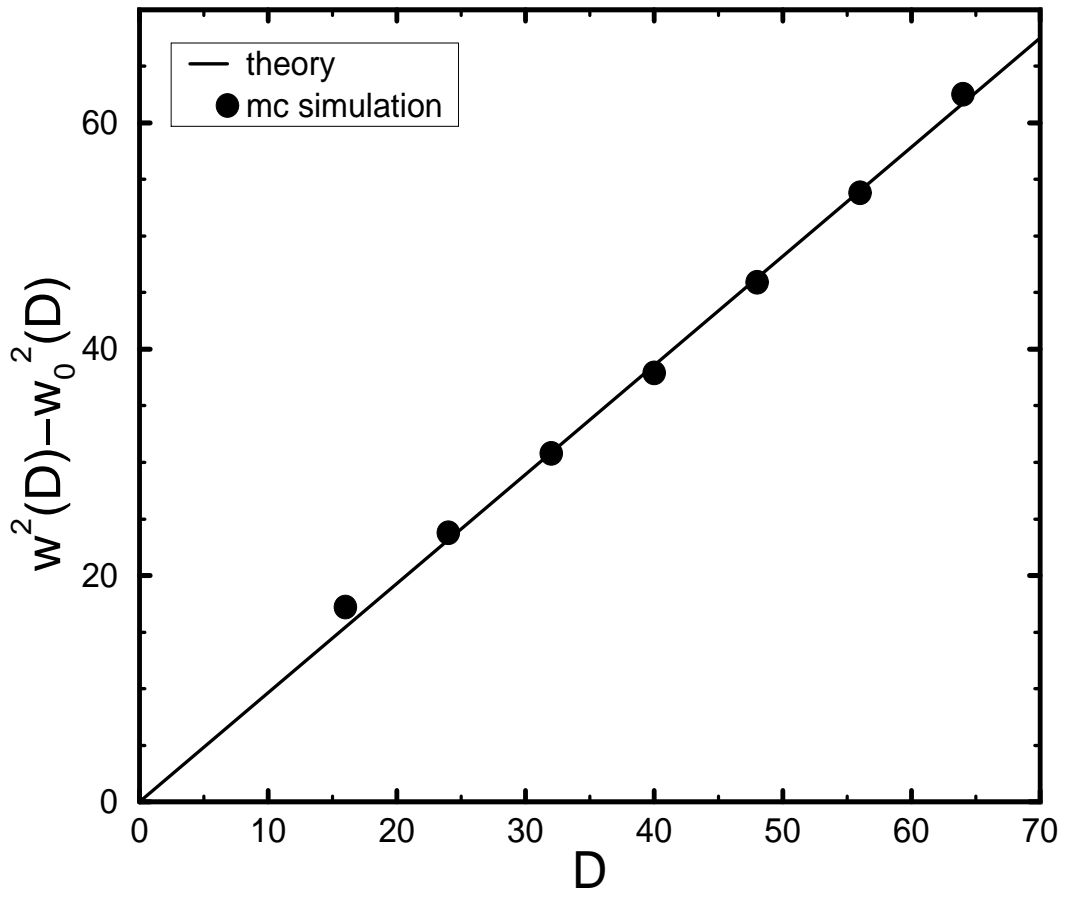


Figure 14
Werner et al
JCP

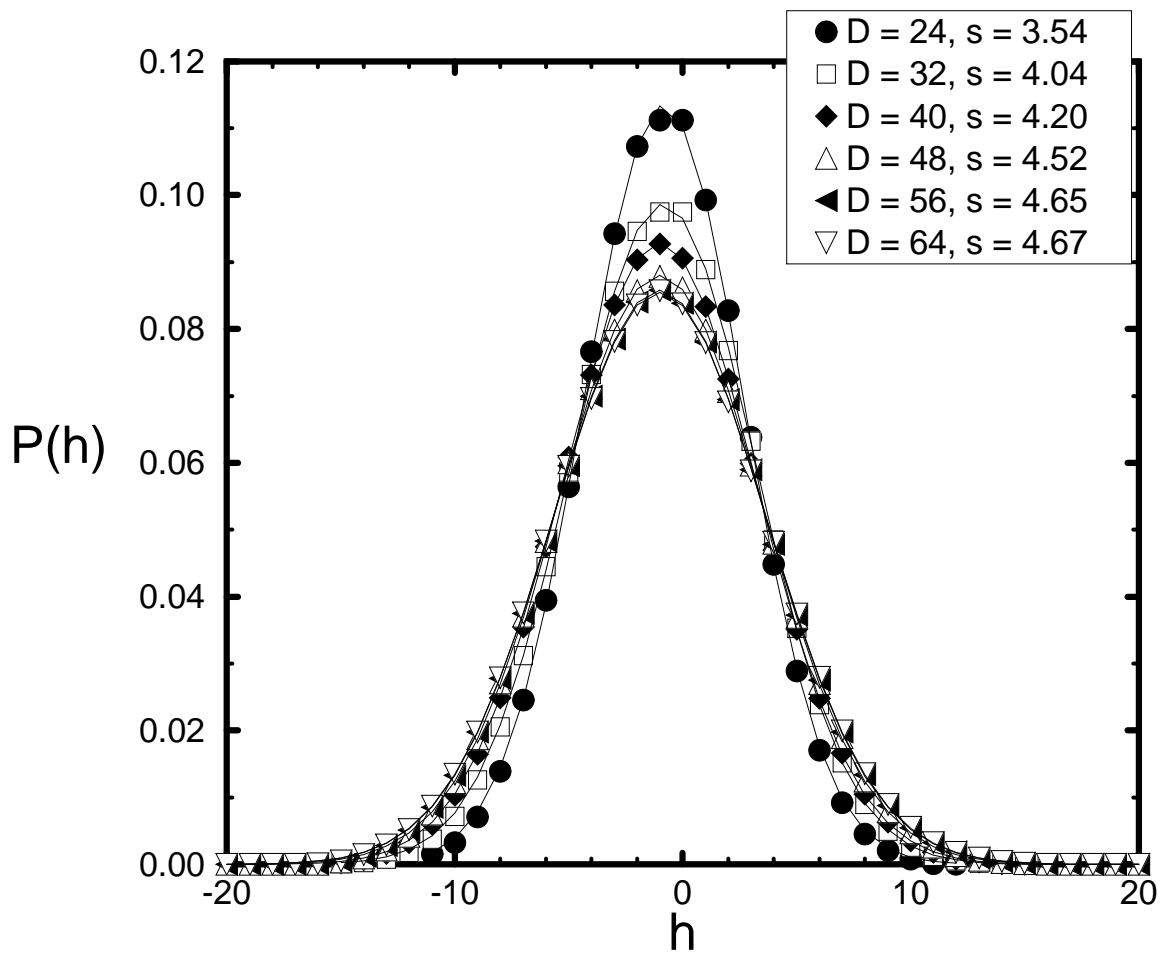


Figure 15
Werner et al
JCP

References

- [1] B.Widom, in *Phase Transitions and Critical Phenomena, Vol.2*, edited by C.Domb and M.S.Green (Academic Press, London 1972), p.79.
- [2] J.S.Rowlinson and B.Widom, *Molecular Theory of Capillarity* (Clarendon Press, Oxford 1982).
- [3] K.Binder, in *Phase Transitions and Critical Phenomena, Vol.8*, edited by C.Domb and J.L.Lebowitz (Academic Press, London 1983), p.1.
- [4] D.Jasnow, Rep.Prog.Phys. **47**, 1059 (1984).
- [5] I.C.Sanchez (ed), *Physics of Polymer Surfaces and Interfaces* (Butterworth-Heinemann, Boston 1992).
- [6] J.W.Cahn and J.E.Hilliard, J.Chem.Phys. **28**, 258 (1958).
- [7] A.Vrij, J.Polym.Sci. Part A2 **2**, 1919 (1968).
- [8] J.F.Joanny and L.Leibler, J.Phys. (Paris) **39**, 951 (1978).
- [9] K.Binder and H.L.Frisch, Macromolecules **17**, 2928 (1984).
- [10] P.G.de Gennes, J.Chem.Phys. **72**, 4756 (1980).
- [11] G.Gompper and M.Schick, Phys.Rev.Lett. **62**, 1647 (1989).
- [12] F.Schmid and M.Schick, Phys.Rev.E **48**, 1882 (1993).
- [13] E.Helfand and Y.Tagami, J.Chem.Phys. **56**, 3592 (1972); *ibid* **57**, 1812 (1972).
- [14] E.Helfand, J.Chem.Phys. **62**, 999 (1975); E.Helfand and A.M.Sapse, J.Chem.Phys. **62**, 1327 (1975).
- [15] J.Noolandi and K.M.Hong, Macromolecules **15**, 482 (1982); K.M.Hong and J.Noolandi, Macromolecules **14**, 727 (1981); *ibid* **16**, 1083 (1983).
- [16] E.Helfand, S.M.Bhattacharjee, and G.H.Fredrickson, J.Chem.Phys. **91**, 7200 (1989).
- [17] K.R.Shull and E.J.Kramer, Macromolecules **23**, 4769 (1990); K.R.Shull, Macromolecules **25**, 2122 (1991); *ibid* **26**, 2346 (1993).
- [18] D.Broseta, G.H.Fredrickson, E.Helfand, and L.Leibler, Macromolecules **23**, 132 (1990).
- [19] K.R.Shull, A.M.Mayes, and T.P.Russell, Macromolecules **26**, 3929 (1993).
- [20] A.N.Semenov, Macromolecules **26**, 6617 (1993); *ibid* **27**, 2732 (1994).
- [21] D.C.Morse and G.H.Fredrickson, Phys.Rev.Lett. **73**, 3235 (1994).

- [22] F.Schmid and M.Müller, *Macromolecules* **28**, 8639 (1995).
- [23] M.Müller, K.Binder, and W.Oed, *J.Chem.Soc.Faraday Trans.* **91**, 2369 (1995).
- [24] D.E.Sullivan and M.M.Telo da Gama, in *Fluid Interfacial Phenomena*, edited by C.A.Croxton (Wiley, New York 1986), p.45.
- [25] M.E.Fisher, *J.Stat.Phys.* **34**, 667 (1984); *J.Chem.Soc.Faraday Trans.* **282**, 1569 (1986).
- [26] S.Dietrich, in *Phase Transitions and Critical Phenomena, Vol.12*, edited by C.Domb and J.L.Lebowitz (Academic Press, London 1988), p.1.
- [27] M.Schick, in *Liquids at Interfaces*, edited by J.Charvolin, J.F.Joanny, and J.Zinn-Justin (North-Holland, Amsterdam 1990), p.415.
- [28] R.Evans, *J.Phys.: Condens.Matter* **2**, 8989 (1990).
- [29] A.O.Parry, *J.Phys.: Condens.Matter* **8**, 10761 (1996).
- [30] E.Blokhuis and B.Widom, *Current Opinion in Colloid & Interface Sci.* **1**, 424 (1996).
- [31] A.O.Parry and R.Evans, *Physica A* **181**, 250 (1992).
- [32] K.Binder, D.P.Landau, and A.M.Ferrenberg, *Phys.Rev.E* **51**, 2823 (1995).
- [33] K.Binder, R.Evans, D.P.Landau, and A.M.Ferrenberg, *Phys.Rev.E* **53**, 5023 (1996).
- [34] T.Kerle, J.Klein, and K.Binder, *Phys.Rev.Lett.* **77**, 1318 (1996).
- [35] M.Müller and A.Werner, *subm. to J.Chem.Phys.*
- [36] In the semi-grand-canonical ensemble, the fluctuations of the average interfacial position \bar{h} in a configuration are according to Eq.28 given by

$$\langle \bar{h}^2 \rangle = \frac{\xi_{||}^2}{L^2 \sigma}.$$

For $L \rightarrow \infty$, this contribution vanishes, and both canonical and semi-grand-canonical ensemble yield the same interfacial width. For finite L , however, the fluctuations of the average position increase the width. In the limit $L \ll \xi_{||}$, $\langle \bar{h}^2 \rangle$ is of the order of D^2 itself, and thus $w = D/2$ for $L/\xi_{||} \rightarrow 0$.

- [37] A.Budkowski, U.Steiner, and J.Klein, *J.Chem.Phys.* **97**, 5229 (1992).
- [38] M.Stamm and D.W.Schubert, *Annu.Rev.Mater.Sci.* **25**, 325 (1995).
- [39] H.J.Leamy, G.H.Gilmer, K.A.Jackson, and P.Bennema, *Phys.Rev.Lett.* **30**, 601 (1973).
- [40] J.Alejandre, D.J.Tildesley, and G.A.Chapela, *J.Chem.Phys.* **102**, 4574 (1995).

- [41] T.L.Hill, *Thermodynamics of Small Systems* (Benjamin, New York 1963).
- [42] We call a mixture symmetric if its Hamiltonian (and hence its free energy) in the bulk is invariant against an interchange of A and B. This is the case e.g. for the Ising spin model of binary mixtures (for zero “magnetic field” the Hamiltonian $\sum_{\langle i,j \rangle} J_{ij} S_i S_j$ is invariant against a reversal of the signs of all spins S_i which may take values $S_i = \pm 1$, the two signs corresponding to lattice sites i being taken by A and B, respectively). “Antisymmetric walls” mean in the Ising spin representation that the wall magnetic fields $H^{(l)}(z)$, $H^{(r)}(z)$ due to the left (right) walls satisfy the condition $H^{(l)}(z) = -H^{(r)}(D - z)$, choosing the z-axis normal to the interface, and the origin at the left wall in Fig.1a.
- [43] K.Binder, P.Nielaba, and V.Pereyra, Z.Physik B: Condens.Matter, in press (1997).
- [44] H.E.Hermes, D.G.Bucknall, and J.S.Higgins, Polymer **38**, 985 (1997).
- [45] F.Schmid and K.Binder, Phys.Rev.B **46**, 13553 (1992).
- [46] G.S.Grest, M.-D.Lacasse, K.Kremer, and A.M.Gupta, J.Chem.Phys. **105**, 10583 (1996).
- [47] T.Kerle et al., to be published.
- [48] I.Carmesin and K.Kremer, Macromolecules **21**, 2819 (1988).
- [49] H.-P.Deutsch and K.Binder, J.Chem.Phys. **94**, 2294 (1991).
- [50] H.-P.Deutsch and K.Binder, Macromolecules **25**, 6214 (1992).
- [51] M.Müller and K.Binder, J.Phys.II (Paris) **6**, 187 (1996).
- [52] K.Binder, in *Monte Carlo and Molecular Dynamics Simulations in Polymer Science*, edited by K.Binder (Oxford University Press, New York 1995), p.1.
- [53] W.Paul, K.Binder, D.W.Heermann, and K.Kremer, J.Phys.II (Paris) **1**, 37 (1991).
- [54] G.S.Grest, M.-D.Lacasse, K.Kremer, and A.M.Gupta, J.Chem.Phys. **105**, 10583 (1996).
- [55] P.J.Flory, *Principles of Polymer Chemistry* (Cornell University Press, Ithaca 1953).
- [56] K.Binder, Adv.Polymer Sci. **112**, 181 (1994).
- [57] J.S.Wang and K.Binder, J.Chem.Phys. **94**, 8537 (1991).
- [58] J.D.Weeks, in *Ordering in Strongly Fluctuating Condensed Matter Systems*, edited by T.Riste (Plenum Press, New York 1980), p.293.
- [59] M.Napiorkowsky and S.Dietrich, Z.Phys.B **89**, 263 (1992); Phys.Rev.E **47**, 1836 (1993).

- [60] C.J.Boulter and A.O.Parry, Phys.Rev.Lett. **74**, 3403 (1995).
- [61] A.O.Parry and C.J.Boulter, Physica A **218**, 77 (1995).
- [62] C.J.Boulter and A.O.Parry, Physica A **218**, 109 (1995).
- [63] A.O.Parry, C.J.Boulter, and P.S.Swain, Phys.Rev.E **52**, 5768 (1995).
- [64] E.Brézin, B.I.Halperin, and S.Leibler, Phys.Rev.Lett. **50**, 1387 (1983).
- [65] R.Lipowsky, D.M.Kroll, and R.K.Zia, Phys.Rev.B **27**, 4499 (1983) .
- [66] D.S.Fisher and D.A.Huse, Phys.Rev.B **32**, 247 (1985).
- [67] R.Lipowsky and M.E.Fisher, Phys.Rev.B **36**, 2126 (1987).
- [68] M.E.Fisher and A.J.Jin, Phys.Rev.B **44**, 1430 (1991); Phys.Rev.Lett. **69**, 792 (1992).
- [69] A.J.Jin and M.E.Fisher, Phys.Rev.B **47**, 7365 (1993); *ibid* B **48**, 2642 (1993).
- [70] M.E.Fisher, A.J.Jin, and A.O.Parry, Ber.Bunsenges.Phys.Chem. **98**, 357 (1994).
- [71] M.E.Fisher and H.Wen, Phys.Rev.Lett. **68**, 3654 (1992).
- [72] P.G.de Gennes, J.Phys.Lett. (Paris) **38**, 441(1977); J.F.Joanny, J.Phys.A:Math.Gen. **11**, L117 (1978).
- [73] K.Binder, J.Chem.Phys. **79**, 6387 (1983); Phys.Rev.A **29**, 341 (1984).
- [74] I.Schmidt and K.Binder, J.Phys. (Paris) **46**, 1631 (1985).